In compliance with the
Canadian Privacy Legislation
some supporting forms
may have been removed from
this dissertation.

While these forms may be included
in the document page count,
their removal does not represent
any loss of content from the dissertation.

University of Alberta

Photoinduced Bragg Gratings in Amorphous As_2Se_3 Thin Films

by

Travis Gordon Robinson

A thesis submitted to the Faculty of Graduate Studies and Research in partial fulfillment of the requirements for the degree of **Master of Science**

Department of Electrical and Computer Engineering

Edmonton, Alberta

Fall 2003

National Library
of Canada

Acquisitions and
Bibliographic Services

395 Wellington Street
Ottawa ON K1A 0N4
Canada

Bibliothèque nationale
du Canada

Acquisisitons et
services bibliographiques

395, rue Wellington
Ottawa ON K1A 0N4
Canada

Your file Votre référence
ISBN: 0-612-87870-8
Our file Notre référence
ISBN: 0-612-87870-8

The author has granted a non-exclusive licence allowing the National Library of Canada to reproduce, loan, distribute or sell copies of this thesis in microform, paper or electronic formats.

The author retains ownership of the copyright in this thesis. Neither the thesis nor substantial extracts from it may be printed or otherwise reproduced without the author's permission.

L'auteur a accordé une licence non exclusive permettant à la Bibliothèque nationale du Canada de reproduire, prêter, distribuer ou vendre des copies de cette thèse sous la forme de microfiche/film, de reproduction sur papier ou sur format électronique.

L'auteur conserve la propriété du droit d'auteur qui protège cette thèse. Ni la thèse ni des extraits substantiels de celle-ci ne doivent être imprimés ou aturement reproduits sans son autorisation.

Canada

University of Alberta

Library Release Form

Name of Author: **Travis Gordon Robinson**

Title of Thesis: **Photoinduced Bragg Gratings in Amorphous As_2Se_3 Thin Films**

Degree: **Master of Science**

Year this Degree Granted: **2003**

Permission is hereby granted to the University of Alberta Library to reproduce single copies of this thesis and to lend or sell such copies for private, scholarly, or scientific research purposes only.

The author reserves all other publication and other rights in association with the copyright in the thesis, and except as hereinbefore provided, neither the thesis nor any substantial portion thereof may be printed or otherwise reproduced in any material form whatever without the author's prior written permission.

Date: 23/09/03

University of Alberta

Faculty of Graduate Studies and Research

The undersigned certify that they have read, and recommend to the Faculty of Graduate Studies and Research for acceptance, a thesis entitled **Photoinduced Bragg Gratings in Amorphous As_2Se_3 Thin Films** submitted by **Travis Gordon Robinson** in partial fulfillment of the requirements for the degree of **Master of Science**.

Dr. F. A. Hegmann

Date: 23/09/03

Abstract

This thesis studies holographic Bragg gratings induced in thermally evaporated thin films of the chalcogenide glass, As_2Se_3. Sub-micron gratings were created using a 10 mW Helium-Neon laser in an interferometric setup. Refractive index modulations as large as 0.036 were recorded in the gratings.

Chalcogenide glasses display several properties that are potentially useful in integrated optics. One property is photodarkening, which is accompanied with a change in the refractive index of the glass. This thesis shows how photodarkening is utilized to create Bragg gratings in the glass, as well as its technological importance.

To my parents, Gordie and Barbara, and to unconditional love

Acknowledgments

The author wishes to thank Dr. Ray DeCorby and Dr. Chris Haugen for their assistance in choosing a research topic, as well as their knowledge and encouragement to see the research through.

I would also like to thank Dr. Safa Kasap and Dancho Tonchev at the University of Saskatchewan, for their expertise and assistance in thin films. This includes their generosity in donating thin film samples to us.

I am indebted to David Clegg, for valuable and practical advice relating to electrical engineering research, and for his expertise in the laboratory.

I also wish to thank the entire photonics group at TRLabs for making my time there both educational and amusing.

I owe a large debt of gratitude to my parents, for their love and support.

Finally, I would like to thank the financial support of TRLabs, and the University of Alberta, which facilitated this research. The working environment provided by TRLabs was excellent, and my experience was very rewarding.

Table of Contents

1. Introduction **1**

1.1. Optical Fiber Communication: Overview 1

1.2. Economic Statistics: Fiber Optic Communication 2

1.3. Next Generation Networks: Integrated Optics 5

1.4. Add-Drop Multiplexor 7

1.5. Outline of Thesis 8

2. Chalcogenide Glasses: Background **9**

2.1. Properties for Integrated Optics 9

2.2. Structure 9

2.3. Band gap 10

2.4. Absorption Edge 11

2.5. Photodarkening 14

2.6 Photoinduced structural changes 17

2.7. Other photoinduced observations 21

2.7.1. Refractive index changes 22

2.7.2. Photoluminescence (PL) 23

2.7.3. Photoconductivity 23

2.7.4. AC conductivity 24

2.7.5. Anisotropy 24

2.7.6. Oscillator behavior 24

2.7.7. Photoamorphization 25

2.7.8. Photodiffusion (Photodoping) 26

2.7.9. Volume change 26

2.8. Gratings 27

2.9. Summary 28

3. Holographically Induced Bragg Gratings: Theory and Experimental Setup 29

3.1. Theory of holographically induced gratings 29

3.2 Characterization of Bragg gratings using diffracted beams 32

3.3 Grating writing experiment 35

3.4. As_2Se_3 Chalcogenide Glass Samples 38

4. Results and Discussion 39

4.1. Diffraction efficiency measurements 39

4.2. Graphing with respect to energy 44

4.3. Related experiments 46

4.4. Additional experimental observations and difficulties 48

4.5 Thermal and Illumination related degradation of photo-induced gratings 51

4.6. Verification of Assumptions 53

4.7. Error Analysis 54

5. Discussion and Future Work 56

5.1. Discussion 56

References 58

Appendix A: Experimental Equipment 64

Appendix B: Swanepoel method for determining refractive index of thin films 65

List of Figures

Figure 1.1. Loss profile of a single-mode silica fiber [1]..... 2

Figure 1.2. Capital expenditure data for the ICT Sector in Canada. The individual groups shown are the Communication Equipment manufactures, the total ICT manufacturing industries, and the Telecommunication service industries [2]..... 3

Figure 1.3. Revenue data for the ICT sector in Canada. Included are the Communication Equipment manufacturing industries and the Communication Service industries [2]..... 3

Figure 1.4. Expenditure data in Research and Development for the ICT sector in Canada. The two groups included are for the Communication Equipment and the entire ICT Sector [2]..... 4

Figure 1.5. Schematic Diagram of Add-Drop Multiplexor..... 7

Figure 1.6. ADM Drop operation..... 7

Figure 1.7. ADM Add operation..... 8

Figure 2.1. Schematic diagrams of two-dimensional atomic structures of the (a) crystalline and (b) amorphous forms of a chalcogenide alloy such as As_2Se_3. The amorphous structure is described as a Continuous Random Network (CRN)..... 10

Figure 2.2 (a) Density of states diagram for crystalline material. The band-gap is shown between E_V and E_C..... 11

Figure 2.2 (b) Density of states diagram for an amorphous material such as As_2S_3. The localized and delocalized states are shown shaded and unshaded respectively. The mobility gap is located between E_V and E_C..... 11

Figure 2.3. Absorption edge of a-As_2S_3 is compared with the absorption edge of c-As_2S_3. Two polarization directions are shown for c-As_2S_3 [12]..... 12

Figure 2.4. The dependence of absorption on photon energy in a-As_2S_3. These plots are commonly used to define the optical gap E_g^{opt}. The two lines on the graph are for as-deposited (right) and photodarkened (left) glass[12]..... 13

Figure 2.5. Urbach edges for several chalcogenide glasses. [14]..... 14

Figure 2.6. Absorption coefficient of (a) evaporated As_2S_3 and (b) evaporated As_2Se_3 [19]. Comparisons are made between as-deposited samples and exposed samples in both cases..... 15

Figure 2.7. X-ray diffraction pattern showing the reversible change in the first sharp diffraction peak of an a-As_2S_3 film [31]..... 18

Figure 2.8. Photoinduced absorption edge shift (at saturation) for evaporated (EV) and melt-quenched (MQ) samples of (a) As_2S_3 and (b) As_2Se_3 as a function of photon energy of exciting light. The edge shift is normalized to the number of absorbed photons. The absorption edges are also shown prior to illumination [16]..... 19

Figure 2.9. Photoinduced edge shift as a function of nt for different incident photon flux n. $\Delta\lambda$ is wavelength shift corresponding to $\alpha = 3 \times 10^4\ cm^{-1}$. The film used was evaporated As_2S_3 with a thickness of 0.344μm, and the excitation energy was 2.877eV [16]..... 20

Fig 2.10. Configuration coordinate diagram used to describe mechanisms behind photodarkening in amorphous materials. Illumination near the band-gap energy (hν) raises electrons from the ground state (I) to the transient state (II). The metastable state (III) is reached after the change in the structure of the glass, which is represented as a change in the configuration coordinate, q. This structure is maintained provided the barrier energy, W, is not reached. 21

Figure 2.11. Oscillating transmission curves for film of $GeSe_2$. Films were illuminated with a 30 mW Helium-Neon laser with different intensities. Top graph is for illumination intensity of 1.66 kW cm^{-2}, bottom graph is for illumination intensity of 2.6 kW cm^{-2} [47]. 25

Figure 3.1. Top view of a Bragg grating, as used in a waveguide structure. Communication data on multiple wavelength carriers propagate from left to right, but at the grating the Bragg wavelength is reflected and will not be part of the output data. 29

Figure 3.2. An interference pattern created by two coherent light beams can be used in light sensitive materials to induce gratings. The writing beams have intensities I_A and I_B, wavevectors k_A and k_B, wavelengths λ_w and interfere at an angle θ. The resulting grating has a grating vector, q. 30

Figure 3.3. Gratings can be detected by transmitting a probe beam (a) perpendicular to the glass surface or (b) at its Bragg angle. The probe beam is diffracted at the angles Φ. 32

Figure 3.4. Setup to write and probe Bragg gratings on Chalcogenide glass thin films. 36

Figure 3.5. Photograph of setup to write and probe Bragg gratings on Chalcogenide glass thin films. 37

Figure 3.6. Photograph of As_2Se_3 glass sample in a holder being illuminated with He-Ne laser. 38

Figure 4.1. Microscopic photograph of a grating photoinduced in a-As_2Se_3 thin film. 40

Figure 4.2. Diffraction efficiency plotted in real time during illumination, for several gratings written at different locations on a single As_2Se_3 sample. 40

Figure 4.3. Diffraction efficiency plots probed during illumination at various locations on the same a-As_2Se_3 thin film sample. Film thickness varied from 1.18 μm to 1.21 μm, as determined by profilometer measurements. The intensity in each arm was ≈ 0.382 mW/mm^2. 41

Figure 4.4. Grating Δn versus illumination time for several gratings located on the same a-As_2Se_3 thin film, with the local film thickness taken into account. Film thickness varies from 1.18 μm to 1.21 μm. 42

Figure 4.5. Diffraction efficiency plots probed during illumination at various locations on a single a-As_2Se_3 thin film sample. Film thickness varied from 2.10 μm to 2.43 μm. 43

Figure 4.6. Grating Δn versus illumination time for several gratings located on the same a-As_2Se_3 thin film. Film thickness varies from 2.10 μm to 2.43 μm. 44

Figure 4.7. Grating Δn versus energy dose for Bragg gratings induced on thin film ranging in thickness from 1.18 μm to 1.21 μm. Peak grating strength occurs in all gratings around an applied energy dose of 225 mJ/mm^2. 45

Figure 4.8. Grating Δn versus energy dose for Bragg gratings induced on thin film ranging in thickness from 2.10 μm to 2.43 μm. Peak grating quality occurs in all gratings around an applied energy dose of 500 mJ/mm^2. 46

Figure 4.9. Absorption coefficient of As_2Se_3 over the visible to near infrared wavelength range. 47

Figure 4.10. Diffraction efficiency graph comparing typical diffraction plot with two atypical plots. The inconsistencies were assumed to be caused by poor surface quality. 49

Figure 4.11. Diffraction efficiency graph comparing gratings written with unequal writing beams and those with equal writing beams. Note that the higher peak diffraction efficiency in the first case is attributable to a greater film thickness. 49

Figure 4.12. Graphs of Δn versus illumination time comparing gratings written with unequal and equal writing beam powers 50

Figure 4.13. Diffraction efficiency graph with points taken over a period of 6 weeks. 51

Figure 4.14. Diffraction efficiency graph comparing gratings written on high intensity white light photodarkened glass and unexposed glass. 52

Figure A.1. Wedge shaped thin film model. 65

List of Tables

Table 2.1 Optical band-gaps of various chalcogenide glasses.....14

Table A.1. List of optical equipment used in experiment.....64

List of Abbreviations

ADM	Add-Drop Multiplexor
As_2S_3	Arsenic Trisulfide
As_2Se_3	Arsenic Triselenide
AWG	Arrayed Waveguide Gratings
ChG	Chalcogenide Glasses
CRN	Continuous Random Network
CW	Continuous Wave
EDFA	Erbium-Doped Fiber Amplifier
EV	Evaporated
GaAs	Gallium Arsenide
He-Ne	Helium-Neon
IC	Integrated Circuit
ICT	Information and Communications Technology
InP	Indium Phosphide
IO	Integrated Optics
LP	Linear Polarizer
MQ	Melt-Quenched
PB	Photobleaching
PD	Photodarkening or Photodetector (Chapter 3)
PL	Photoluminescence
S	Sulfur
Se	Selenium

SOI	Silicon on Insulator
Te	Tellurium

Chapter 1

Introduction

1.1. Optical Fiber Communication: Overview

The telecommunication industry has come a long way in the last several decades since the move to optical fiber as a transmission media in 1980. The first lightwave systems operated around the wavelength of 0.8 μm. Loss at this wavelength was still high (3 dB/km), and although 0.8 μm sources are still used in short range communication, long haul communication subsequently moved to wavelengths in the range of 1.3 μm where the loss is below 1 dB/km. Single mode fibers were introduced to compensate for dispersion-induced bit-rate limitations. The loss profile of silica fiber is shown in Figure 1.1. The minimum loss occurs at around 1.55 μm, and this is the wavelength region used for the current generation of optical systems. Recent work has been done to remove the loss peak around 1.4 μm, which is caused by hydroxyl impurities in the glass. This has opened up a large operational region extending from the 1.3 μm range to the 1.55 μm range. Another major advancement was the development of optical amplifiers, which greatly reduced the need for numerous repeaters along a fiber span. The most widely used amplifier is the erbium-doped fiber amplifier (EDFA), which is pumped with 980 nm or 1480 nm light from semiconductor laser sources, and amplifies signals in the 1550 nm range.

The major driving force behind the great expansion of fiber optic development in the last decade has been the growing worldwide use of the Internet. The Internet is used by millions of people everyday to conduct their shopping and banking activities. People also log on to gamble, chat on-line, visit news sites, or use a multitude of other services provided on the World Wide Web. The Internet growth has stalled in the past couple of years (2001-2003), but this situation is expected to be temporary.

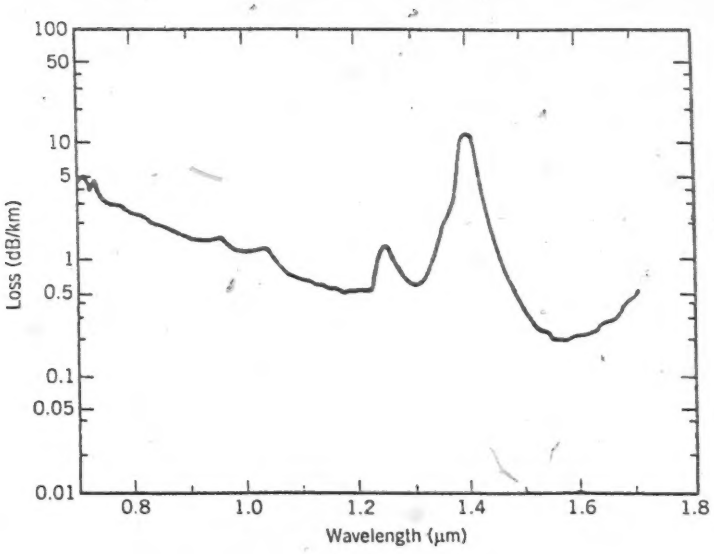

Figure 1.1. Loss profile of a single-mode silica fiber [1].

1.2. Economic Statistics: Fiber Optic Communication

To better understand the current state of the telecommunication industry, Figures 1.2 to 1.4 display various economic data obtained from Statistics Canada pertaining to the information and communications technology (ICT) sector [2]. This sector includes manufacturing and sales of goods and services for information processing and communication. The sector can be broken down into several subdivisions, including communication equipment manufacturing and communication services. The following data was last updated in November 2002.

Figure 1.2 shows the capital expenditures over the past eight years for the communication equipment manufacturers, the total ICT manufacturing industries (which include the communication equipment manufacturers), and the telecommunication service industries. All values are referenced to 1995. Both manufacturing indices peaked in the year 2000 after a substantial rise, then dropped off considerably. The communication equipment manufacturing expenditures have dropped 20% from its year 2000 value of $893 Million.

However in 2002 the expenditures in this industry remained the same as year 2001 at $715 Million. The telecommunication service decline started after the year 2001.

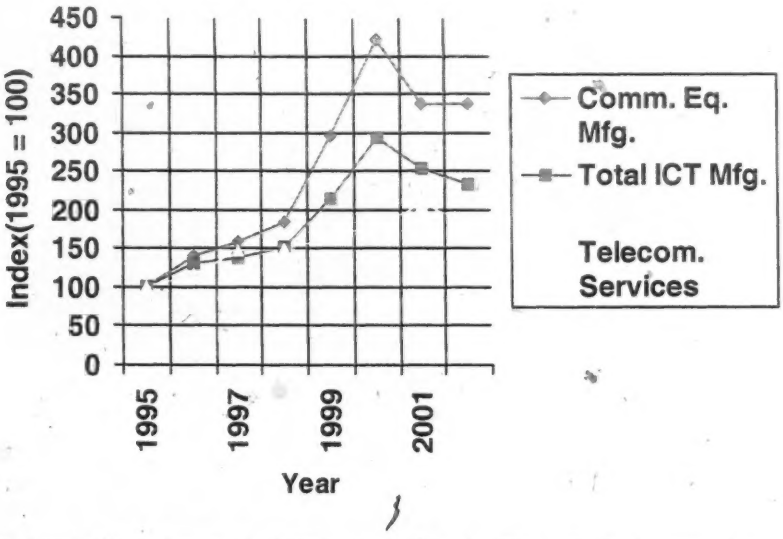

Figure 1.2. Capital expenditure data for the ICT Sector in Canada. The individual groups shown are the Communication Equipment manufactures, the total ICT manufacturing industries, and the Telecommunication service industries [2].

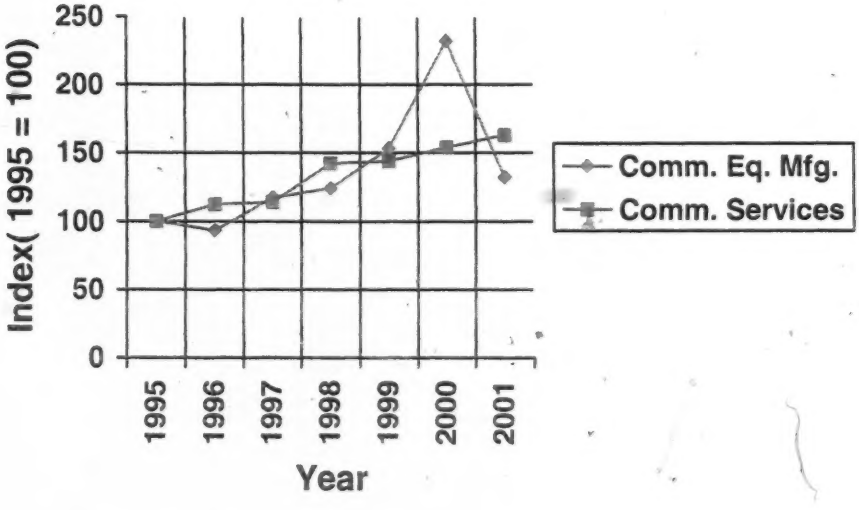

Figure 1.3. Revenue data for the ICT sector in Canada. Included are the Communication Equipment manufacturing industries and the Communication Service industries [2].

Figure 1.3 shows the revenue generated by both the communication equipment manufacturing industry and communication service industry. Revenue data was referenced to 1995, and data for the year 2002 was not available when this thesis was written. As expected, in the year 2001 there was a huge drop in revenue generated by equipment makers to $9.6 Billion from $16.9 Billion. The service industry continued to show increased revenue in 2001 to $32.8 Billion from $31.1 Billion in 2000.

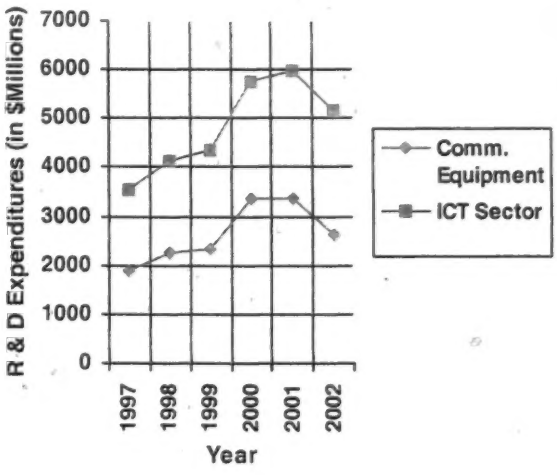

Figure 1.4. Expenditure data in Research and Development for the ICT sector in Canada. The two groups included are for the Communication Equipment and the entire ICT Sector [2].

Figure 1.4 shows the money spent for research and development in both the entire ICT sector, and for the communication equipment sector alone. The money spent researching communication equipment constitutes roughly half the money spent in the entire sector. Total expenditures on research dropped off considerably in the year 2002. Expenditures on equipment research dropped off from $3.4 Billion to $2.6 Billion.

It is obvious from Figures 1.2 to 1.4 that the communication industry has taken a step back from its phenomenal climb in the late 1990s. However, with tens of billions of dollars still flowing through telecommunication service companies (in Canada), equipment manufacturers continue to have a significant market for their products. It is also clear that considerable money is still spent on research and development.

Companies may simply have to be quite selective in what products are to be researched in the future.

1.3. Next Generation Networks: Integrated Optics

It is widely believed that the optical communication industry has been hampered by low levels of device integration. Traditionally, discrete devices (amplifiers, multiplexers, repeaters, sources, detectors) are manufactured separately, and subsequently packaged together. In integrated optics (IO), the goal is to manufacture numerous devices on a single monolithic substrate. This improves the effectiveness and reliability of their interconnections and lower the overall manufacturing cost.

Technology used in optical devices fall in one of two categories: active or passive. Active devices require some form of input to control their operation, whereas passive devices do not. Examples of active device technology include semiconductor lasers and rare earth doped optical amplifiers. Examples of passive device technology include arrayed waveguide gratings (AWGs), thin film filters, photonic crystals, and Bragg gratings. Combining several passive and/or active technologies allows complex sub-systems to be manufactured, such as Add/Drop Multiplexers, gain flattening filters, and optical receivers. The goal of IO is to combine several devices manufactured in compatible material systems on a single platform or substrate. In the same way electronic integrated circuits (ICs) are created using a silicon platform, integrated optics can be realized by using a multifunctional optical material system as the underlying platform.

The search for a universal integrated optical material will probably never be complete, because every material has its benefits and drawbacks. No single material offers the full range of active and passive functionality required for photonic devices, but there are several materials that draw the main interest of developers of integrated optical devices. The most widely used passive waveguiding technology employs silica glass on silicon substrates [3]. In the last few years there has been an increased interest in using silicon

on insulator (SOI), as a waveguiding platform [4]. These materials, however, are limited primarily to passive devices. Two material systems that can be utilized in both passive and active devices are the InP and GaAs based semiconductors. However, these material systems are relatively complex and costly to manufacture. Chalcogenide glasses are an interesting alternative, which can potentially enable both passive and active device functions, and be manufactured at low-cost on arbitrary substrates.

Chalcogenide glasses (ChG) are amorphous compounds containing one or more elements from the Chalcogen group (6A) of the periodic table, specifically Sulfur (S), Selenium (Se), and Tellurium (Te). Oxygen is not included in this group because it has somewhat different properties, and oxide glasses are generally classed separately. Chalcogenide glasses have many attributes that make them extremely beneficial to integrated optics. They are transparent throughout the entire mid-infrared region including the communication wavelengths of 1300 nm and 1550 nm, have displayed large optical non-linearities, have relatively large refractive indices, and can be processed at low temperatures. They also exhibit certain photoinduced changes when illuminated with near band-gap light. The basis of this thesis is a study of photoinduced refractive index changes, which were used to realize Bragg gratings in amorphous As_2Se_3 thin films.

Chalcogenide glasses were first suggested for integrated optic use in 1974 [5], where waveguiding properties were investigated. Losses of 0.1 dB/cm were measured, which was acceptable for IO devices, but long distance communication on chalcogenide fibers was not feasible. Research continued on the properties of such glasses, but no devices were manufactured. In the past decade, there has been a renewed interest in integrated optical devices, and along with it, a renewed interest in chalcogenide glasses. Recent research on chalcogenide glass devices encompasses both active and passive components, including lasers [6], amplifiers [7], switches [8], and waveguides [9].

In this thesis we investigate gratings in As_2Se_3 thin films. Gratings such as these may be integrated in more complex photonic devices, such as an Add-Drop Multiplexor.

1.4. Add-Drop Multiplexor

One eventual device that could be made from the Chalcogenide glass/Bragg grating research discussed in this thesis is an Add-Drop Multiplexor (ADM). This would utilize both the waveguiding property of the glass, as well as its photoinducing properties. ADMs are optical network devices that can add or remove a chosen wavelength to a system that contains multiple wavelengths (channels) of communication. A top view of an Add-Drop Multiplexor is shown in Figure 1.5.

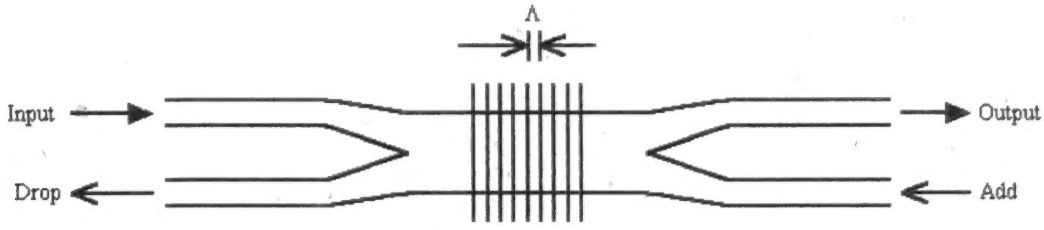

Figure 1.5. Schematic Diagram of Add-Drop Multiplexor.

The ADM is designed so that the optical input signal (top left) is entirely passed through to the output (top right). The middle section consists of a Bragg grating with period Λ. Bragg gratings will be discussed in Chapter 3. Input wavelengths that satisfy the Bragg condition, shown in equation (1.1) are reflected at the grating. All other wavelengths are transmitted through to the output.

$$m\,\lambda_B = 2\,n\,\Lambda\,, \qquad (1.1)$$

λ_B is the Bragg wavelength, m is the order of the grating, n is the refractive index of the waveguide, and Λ is the period of the grating. The reflected waves exit the device through the Drop port as shown in Figure 1.6.

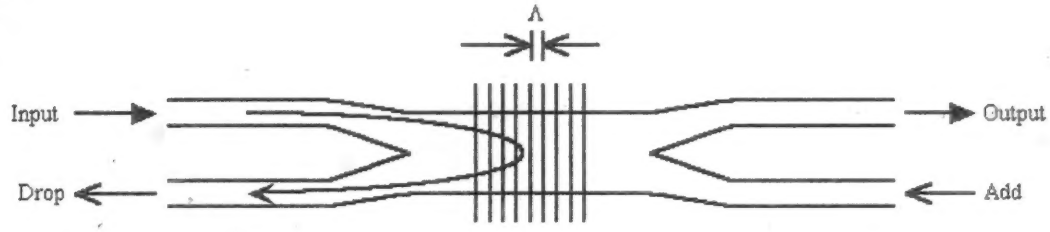

Figure 1.6. ADM Drop operation

Similar to the Drop operation, if the same wavelength λ_B is inputted at the Add port it is reflected by the Bragg grating and added to the signal exiting at the Output port. This is shown in Figure 1.7.

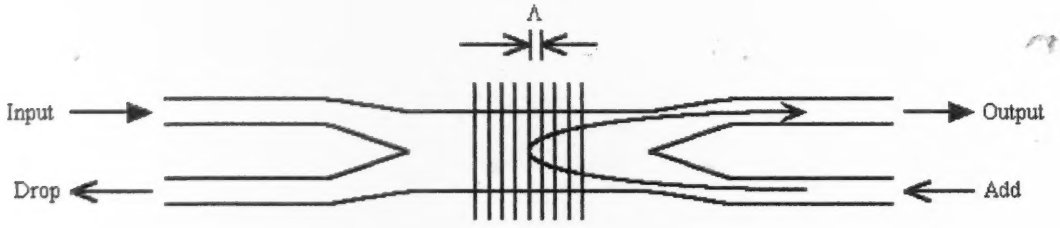

Figure 1.7. ADM Add operation

1.5. Outline of Thesis

Chalcogenide glasses have great potential in the field of integrated optics. One promising characteristic is that Bragg gratings can be directly patterned in ChG thin films. This thesis discusses such gratings produced in a-As_2Se_3. Chapter 2 of this thesis discusses some of the general properties of Chalcogenide glasses, with particular emphasis on photoinduced effects, which include the refractive index change used to produce gratings. Chapter 3 gives a brief description of Bragg gratings, as well as the equations and measurements used to characterize them. This is followed by a description of the experimental setup. Chapter 4 contains results from experimentation. Chapter 5 concludes with a discussion, as well as some recommendations for future work that would further the research discussed throughout this thesis.

Chapter 2

Chalcogenide Glasses: Background

2.1. Properties for Integrated Optics

As mentioned in the previous chapter, Chalcogenide glasses (ChG) are amorphous compounds that contain one or more of the group 6A chalcogen elements (S, Se, Te). These glasses are of interest to communication researchers for their potential applications to integrated optics. Their high refractive indices (n ~2.5 – 3.0), and relatively low losses through the near-to mid-infrared make them attractive waveguiding materials. Chalcogenide glasses have shown large optical nonlinearities, and all-optical switching devices are being investigated. Kerr coefficients of 1000 times those in fused silica have been recently reported [10]. Also, rare-earth doping has been achieved, which has led to amplifier research [11]. Another important property of Chalcogenide glass is its ease of production. Thin chalcogenide films can be deposited with the substrate maintained at room temperature. This allows deposition of Chalcogenide glass on an existing substrate (such as silicon electronics), without subjecting the underlying devices to extreme temperatures.

These properties of Chalcogenide glass are extremely interesting and useful, but it's the photosensitive properties of ChG that form the subject of the present thesis. When Chalcogenide glass is illuminated by band-gap light, or near band-gap light, certain structural changes occur in the glass and its optical properties are modified. These photoinduced changes have received much attention in recent years, and will be the focus of this thesis.

2.2. Structure

Structurally, Chalcogenide glasses differ from their crystalline counterparts in two specific ways. First, there is a significant spread in bond angles in the glass phase.

Second, long range order is not present. Such a structure is described as a continuous-random network (CRN), and Figure 2.1 shows the structural difference between a two dimensional crystalline structure, and a CRN structure. The short range order is the same in both the crystalline structure and the amorphous one. However, in the amorphous structure the order is lost beyond the nearest neighbors.

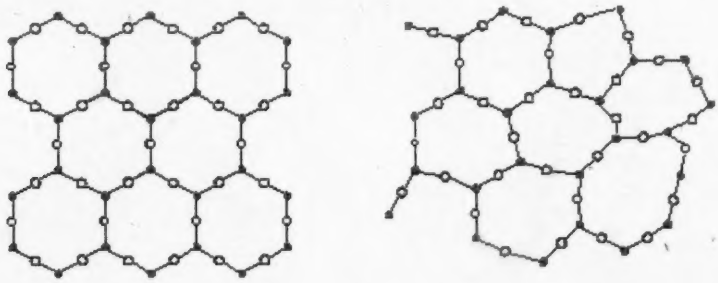

(a) (b)

Figure 2.1. Schematic diagrams of two-dimensional atomic structures of the (a) crystalline and (b) amorphous forms of a chalcogenide alloy such as As_2Se_3. The amorphous structure is described as a Continuous Random Network (CRN).

2.3. Band gap

The density of states diagram for crystalline semiconductors contains two distinct bands (representing the valence and conduction bands), with the forbidden band-gap between them, as shown in Figure 2.2(a). Amorphous materials do not have the sharp band edges, as seen in Figure 2.2(b), because of the inherent disorder present. This disorder gives rise to the shaded tails, which consist of localized states. The carrier mobility in these regions are considerably lower (by a factor of 10^3) than in the delocalized state regions, shown unshaded. This gives rise to a mobility gap between E_v and E_c, which is the amorphous semiconductor equivalent of the crystalline band-gap.

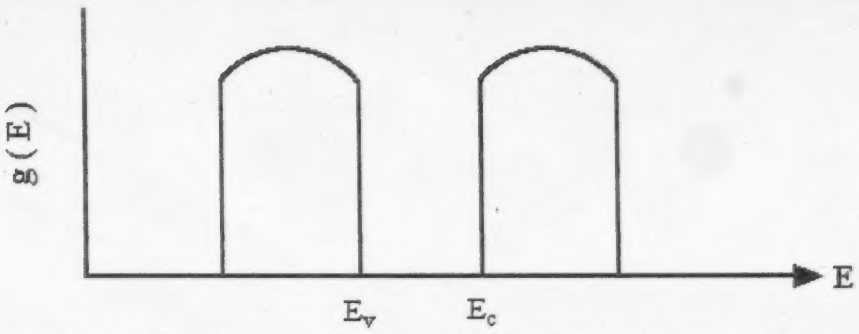

Figure 2.2 (a) Density of states diagram for crystalline material. The band-gap is shown between E_V and E_C.

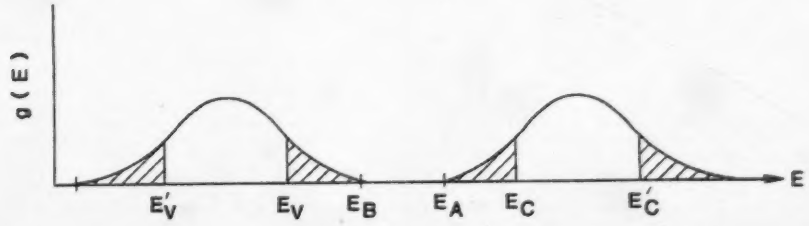

Figure 2.2 (b) Density of states diagram for an amorphous material such as As_2S_3. The localized and delocalized states are shown shaded and unshaded respectively. The mobility gap is located between E_V and E_C.

2.4. Absorption Edge

One of the most important optical properties of an amorphous semiconductor is its absorption edge. Figure 2.3 shows the typical shape of the absorption edge for As_2S_3, and compares the absorption edge of a crystalline (c) structure with an amorphous (a) one. The absorption edge for chalcogenide glasses is composed of three distinct regions. Region A is the high absorption region ($\alpha \geq 10^4$ cm^{-1}). Region B contains the absorption edge itself (1 cm$^{-1} \leq \alpha \leq 10^4$ cm^{-1}), according to the conventional definition [12]. Region C is the weak absorption tail (α<1 cm^{-1}).

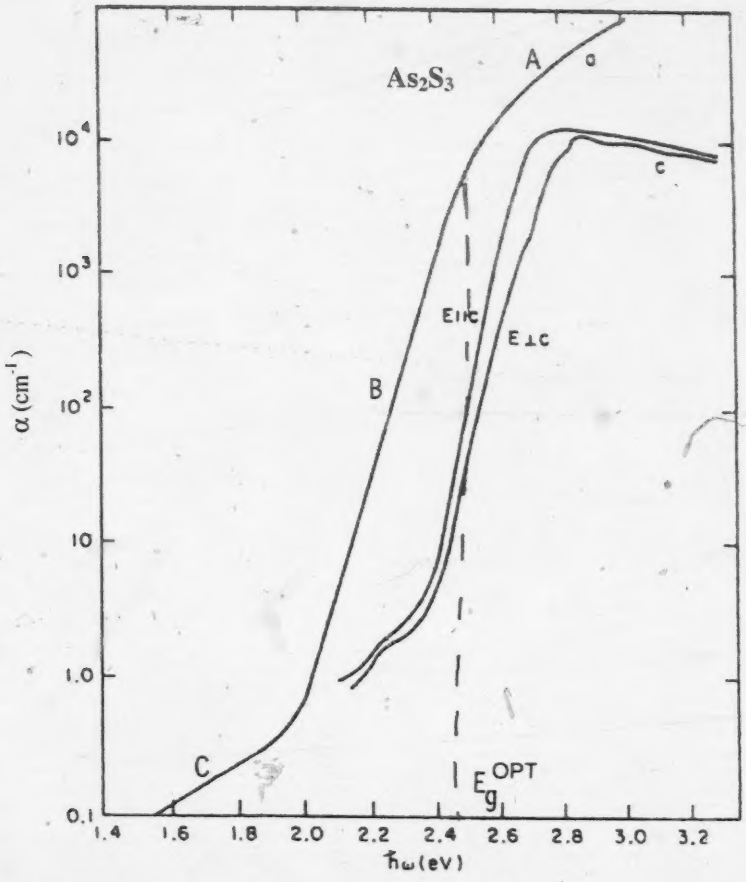

Figure 2.3. Absorption edge of a-As_2S_3 is compared with the absorption edge of c-As_2S_3. Two polarization directions are shown for c-As_2S_3 [12].

In the high absorption region A, the absorption is given by the formula [12],

$$\hbar\omega\alpha(\omega) \sim (\hbar\omega - E_g)^2 . \qquad (2.1)$$

E_g is the optical band-gap of the material, as defined by Tauc [13]. This band-gap is determined by plotting $(\hbar\omega\alpha)^{1/2}$ versus $\hbar\omega$ in region A, and extrapolating the line so that it intersects the horizontal axis. The intersection point defines the so-called Tauc energy gap, often referred to as the optical band-gap. A plot of this kind is shown in Figure 2.4 for As_2S_3.

Region B is named the Urbach tail region and has an energy dependant absorption given by equation (2.2) [13].

$$\alpha(\omega) = \alpha_0 \exp\left[-\Gamma\left(E_1 - h\omega\right)\right] \tag{2.2}$$

E_1 is an energy comparable to E_g, and Γ is a temperature dependant constant. In most amorphous semiconductors, regions A and B of the absorption edge shift together when photodarkened. Figure 2.5 shows the absorption edge in the Urbach region for several chalcogenide glasses. Optical band-gaps for several chalcogenide glasses are shown in Table 2.1.

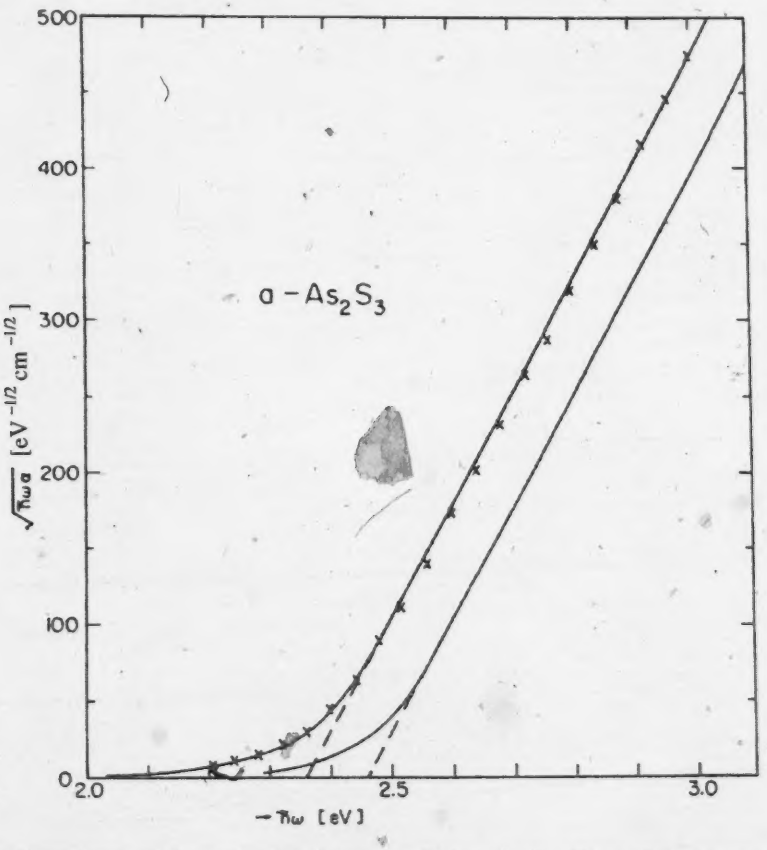

Figure 2.4. The dependence of absorption on photon energy in a-As_2S_3. These plots are commonly used to define the optical gap E_g^{opt}. The two lines on the graph are for as-deposited (right) and photodarkened (left) glass[12].

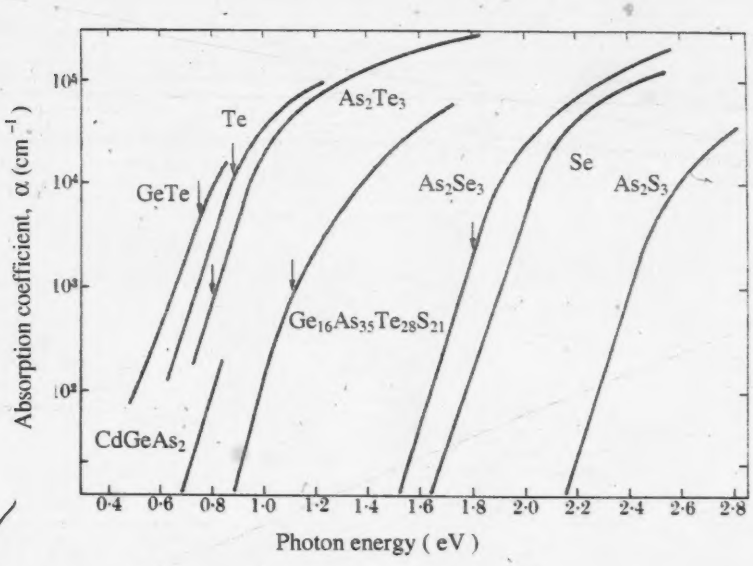

Figure 2.5. Urbach edges for several chalcogenide glasses. [14]

Chalcogenide Glass	Optical Band-gap	Reference
As_2S_3	2.32 eV	[14]
As_2Se_3	1.76 eV	[14]
$As_{24}S_{38}Se_{38}$	2.1 eV	[15]
As_2Te_3	0.83 eV	[14]
$GeSe_2$	2.20 eV	[16]
GeS_2	3.15 eV	[16]
$As_{40}Se_{50}Ge_{10}$	1.57 eV	[16]

Table 2.1 Optical band-gaps of various chalcogenide glasses

2.5. Photodarkening

Photoinduced changes in chalcogenide glass have been reported since 1971, when photodarkening (PD) was first observed [17, 18]. Photodarkening is defined as a red shift in the absorption edge due to illumination at an appropriate wavelength. This is shown in Figure 2.6, where the absorption coefficient, α is plotted versus photon energy.

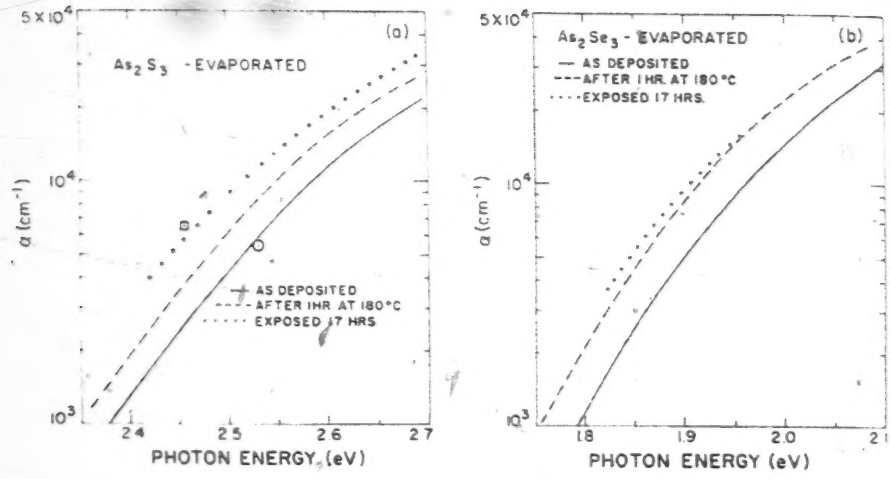

Figure 2.6. Absorption coefficient of (a) evaporated As_2S_3 and (b) evaporated As_2Se_3 [19]. Comparisons are made between as-deposited samples and exposed samples in both cases.

For many chalcogenide glasses, exposure to near band-gap light produces a red-shift in the absorption edge. This effect can be partially reversed by heating the sample near its glass transition temperature, a process known as thermal bleaching. Repeated illumination and heating stages can continually darken and bleach the glass. Figure 2.6 shows that photodarkening is observed in both a-As_2S_3 and a-As_2Se_3, although to different degrees. The light source used to obtain the data in Figure 2.6 [19] was a tungsten filament with a 0.8 μm short wavelength pass filter and an intensity of 0.1 W/cm^2. More common illumination sources for Arsenic-based glasses are argon ion lasers (λ = 488 nm, E= 2.54 eV), (λ = 514.5 nm, E = 2.41 eV) or a helium-neon laser (λ = 633 nm, E = 1.96 eV) [36,62,64,65]. In 1977, Hamanaka et al. observed photodarkening in both evaporated and melt-quenched As_2S_3 [20]. However, crystalline As_2S_3 did not exhibit photodarkening. Thus the widely-held belief is that photodarkening is dependent on the random nature and defect states of a glass.

In 1978, Tanaka varied the content of evaporated As_xS_{100-x} films and reported that for x = 40 both annealed and illuminated annealed films had the same absorption coefficient [21]. This did not apply to other concentrations, so they concluded that for repeatable reversible photodarkening processes the stoichiometric As_2S_3 composition must be used.

In 1980 Tanaka measured the transmission/ absorption of both a-As_2S_3 and a-As_2Se_3, and reported that band-gap illumination was required to shift the absorption edge [16]. However, photodarkening and other photoinduced effects have been observed after sub-band-gap illumination at wavelengths in the Urbach region [22]. The edge shift measured by Tanaka also saturated to similar values for any wavelength of illumination above the band-gap. They noted that this was different from the behavior observed for a-Se and a-S elemental chalcogens [23]. In those glasses, maximum absorption edge shift occurred for wavelengths just above their band-gaps then dropped off with either higher or lower photon energy illumination.

Illumination of a chalcogenide glass with band-gap light does not always lead to photodarkening. Some chalcogenide glasses display photobleaching (PB), which is an absorption edge shift toward higher energies. Generally, Arsenic based glasses photodarken, whereas Germanium based glasses photobleach [24]. Igo also observed that with films of $As_{40}Se_{50}Ge_{10}$, low power laser light caused darkening, whereas high power laser light caused bleaching [25]. There have also been some conflicting reports for the same glass. For example, in contrast to the general rule stated for Ge glasses above, GeS_2 and $GeSe_2$ glasses have also been reported to under go photodarkening in certain circumstances [26].

The degree of shift in the absorption edge has also been shown to be dependent on several factors. High illumination intensity and high exposure energy both appear to raise the amount of photodarkening that takes place [16]. Temperature also affects photodarkening. Tanaka observed that illumination at low temperatures increases the magnitude of the shift. The shift became more pronounced as the temperature is decreased. Low temperature darkening is partially bleached when returned to room temperature, and can also be bleached by illuminating with below band-gap light. At the other extreme, Averyanov et al. showed that illumination at higher temperatures (above room temperature) also increased the degree of absorption edge shift [27].

In 1987, Liu showed that adding small amounts of copper to As_2S_3 or As_2Se_3 glasses can eliminate any photodarkening affect from taking place [28]. Also, films of As_2Se_3 thinner than 50 nm were reported to not exhibit photodarkening [29]. There have also been some studies reporting that pulsed laser illumination is more effective than continuous wave (CW) laser illumination [30]. This result highlights the nonlinear nature of the photo-induced changes. A high-intensity pulsed source induces much larger changes than a CW source, even for comparable energy doses.

2.6 Photoinduced structural changes

The reversible shift in the optical absorption in chalcogenide glasses is accompanied by several other reversible properties as well. These include changes in the refractive index, electron spin resonance and anisotropy, photoconductivity, volume, and the dissolution rate in various etchants. The sum of all these changes led researchers to believe that the photodarkening observed in chalcogenide glasses was due to changes in its structure. This was first proved in 1975 by an x-ray diffraction experiment [31]. Diffraction peaks occur at locations representing the distance between an atom and its nearest neighboring atoms (first diffraction peak), as well as its next nearest atoms (second diffraction peak), and so on. The intensity of these curves represents the number of nearest bonded atoms at a given distance. Tanaka observed that the first sharp peak of annealed a-As_2S_3 underwent reversible changes upon illumination and annealing. Results from this experiment are shown in Figure 2.7. After illumination at temperatures of 290 K or 77 K, the location of the first diffraction peak widened and shifted to the right (higher angle), which represents more variety in the nearest bonding distance, as well as a general increase in the average distance of the first bonded atom. This shift was also accompanied with a general decrease in intensity, although the areas under the curves are approximately the same. This implies that the number of atoms bonded to a given atom is the same as before illumination, but there is more variety in the bonding distance. Upon further annealing, the pattern returned to the original diffraction patterns. The reversible changes in the diffraction patterns was more pronounced when illuminated at

77 K, rather than 290 K. Since the initial results reported by Tanaka, numerous other experiments have verified the reversible nature of chalcogenide glass structures.

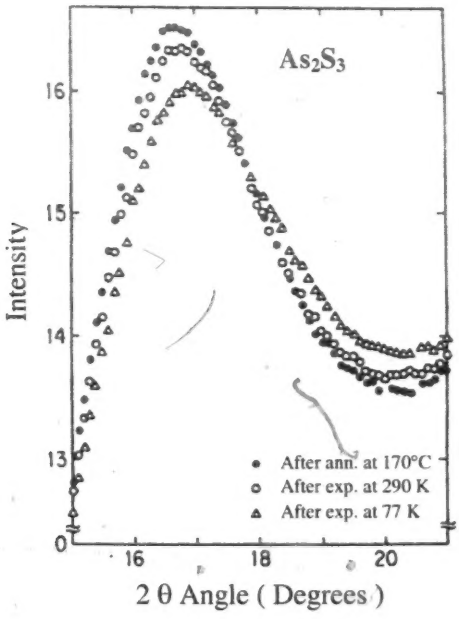

Figure 2.7. X-ray diffraction pattern showing the reversible change in the first sharp diffraction peak of an a-As_2S_3 film [31].

It is worth asking why chalcogenide glasses display such significant structural changes, when most other semiconductors do not. The structural changes that occur in the glass upon photodarkening appear to be dependent on the disordered nature of the glasses themselves. Chalcogenide glasses in crystalline form do not exhibit the photodarkening that characterizes their amorphous counterparts [20]. The photon energies of the exposure light are too small to modify a crystalline structure, whereas amorphous materials are composed of disordered states in several different atomic configurations having local energy minimums. These minimums are close enough together that a photon has enough energy to cause a transition to a different configuration. This said, structural disorder does not guarantee photodarkening. Neither a-As nor a-Si display PD, although a-S and a-Se do [32]. It seems that the chalcogen element itself plays a major role in the structural changes that occur during photodarkening.

The photodarkening of chalcogenide glasses has been studied over the past two decades, but much about the mechanism responsible remains unknown. We can start to understand it by studying the relationship between the change in the optical band gap (ΔE) and the illumination energy. The change in the optical band gap is equivalent to the shift in the absorption edge, and is one way of measuring the magnitude of photodarkening. In 1980 Tanaka [16] plotted the change in the optical band gap as a function of illumination photon energy for As_2S_3 and As_2Se_3. These graphs are displayed in Figure 2.8. It was noted that the minimum photon energy required to induce photodarkening was near the optical band gap. The amount of absorption edge shift was also studied as a function of photon flux and the number of photons absorbed. This is shown in Figure 2.9. The amount of photodarkening increases with both photon flux and the number of photons absorbed, up to differing saturation points.

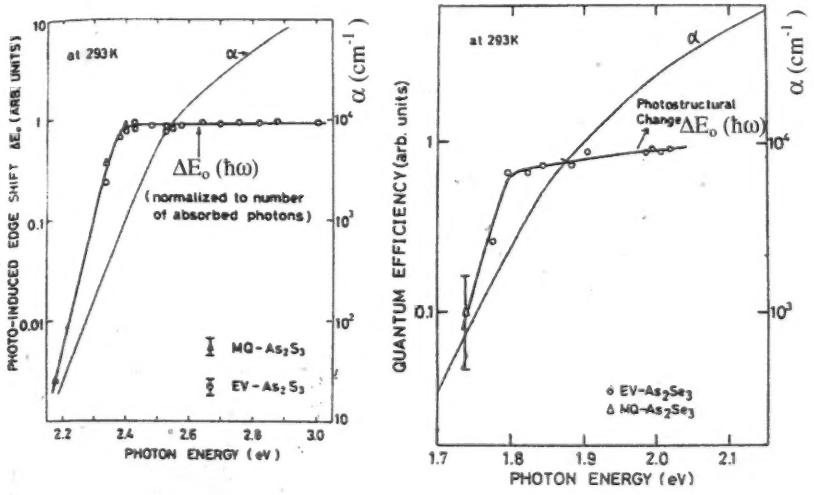

Figure 2.8. Photoinduced absorption edge shift (at saturation) for evaporated (EV) and melt-quenched (MQ) samples of (a) As_2S_3 and (b) As_2Se_3 as a function of photon energy of exciting light. The edge shift is normalized to the number of absorbed photons. The absorption edges are also shown prior to illumination [16].

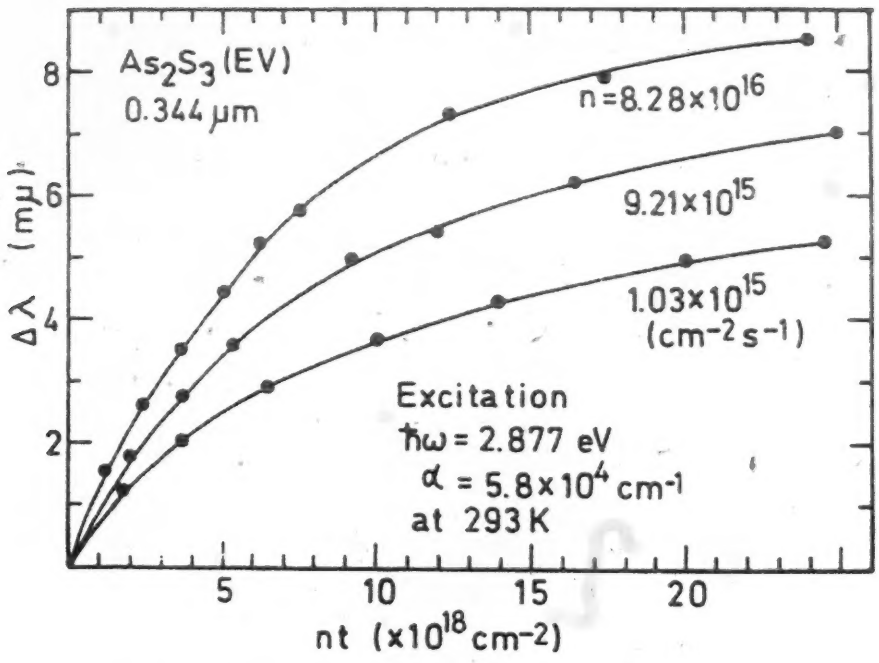

Figure 2.9. Photoinduced edge shift as a function of nt for different incident photon flux n. $\Delta\lambda$ is wavelength shift corresponding to $\alpha = 3 \times 10^4\ cm^{-1}$. The film used was evaporated As_2S_3 with a thickness of 0.344μm, and the excitation energy was 2.877eV [16].

It has already been mentioned that thermally annealing the sample may reverse changes in the structure of the glass. If the deposited sample is annealed prior to illumination the photodarkening/thermal-bleaching cycle may be repeated over and over. The exact mechanisms responsible are the subject of ongoing debate, but several models have been proposed. Many of the models appear as a simplistic configurational coordinate diagram, similar to Figure 2.10. Energy is plotted versus a configurational coordinate, q, which is some measure of the structural change. The diagram shows three states: a ground state (I), a transient excited state (II), and a metastable state (III). Upon illumination (hv), the atom (or atoms) represented here are excited from the ground state (I) to the transient state (II). The metastable state (III), which is of a lower energy than the transient state, is reached by the means of a structural change. This is shown as a change in the configurational coordinate q. W, is the barrier energy that thermally must be exceeded to restore the glass to its initial ground state. This can be achieved by annealing.

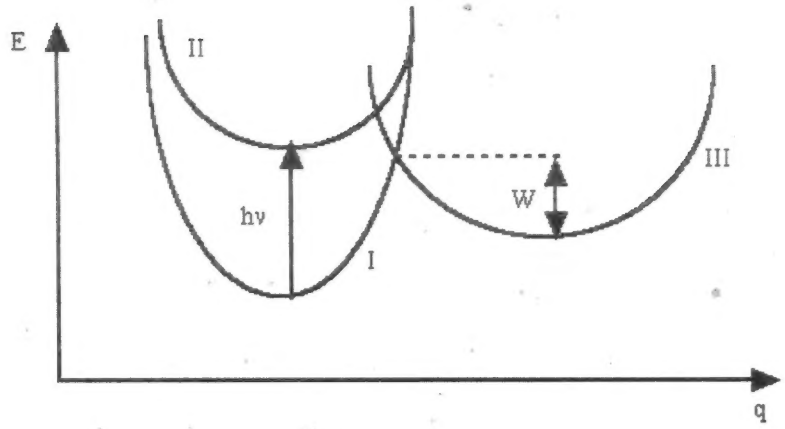

Fig 2.10. Configuration coordinate diagram used to describe mechanisms behind photodarkening in amorphous materials. Illumination near the band-gap energy (hν) raises electrons from the ground state (I) to the transient state (II). The metastable state (III) is reached after the change in the structure of the glass, which is represented as a change in the configuration coordinate, q. This structure is maintained provided the barrier energy, W, is not reached.

One similarity in every study of PD is that the process saturates in all cases. At first, this is counter-intuitive as photodarkening itself is a positive feedback process. When a photon is absorbed, the absorption coefficient is increased. This occurs when the absorption edge shifts to lower energies (photodarkened). With a higher absorption coefficient, more photons will be absorbed and so on. Why then does the PD process always saturate? Many agree with Yang [33] that the photodarkening alters the network structure such that further photodarkening is restricted.

2.7. Other photoinduced observations

Besides photodarkening and photobleaching, several other photoinduced effects have been observed in chalcogenide glasses. Some of the most interesting results reported in the literature are discussed below. Note that some effects have been observed only in particular ChG alloys, and the magnitude of each effect is also alloy-dependent. There

are many factors that may influence the observed characteristics, especially the glass preparation method.

2.7.1. Refractive index changes

Along with the increase in absorption coefficient, which occurs in photodarkening, a chalcogenide glass also demonstrates an increase in its refractive index. This change in the index of refraction is due to its connection with the absorption coefficient via the Kramers-Kronig relations. DeNeufville measured refractive index changes imparted by illumination of unannealed films of As_2S_3 and As_2Se_3 to be 0.107 and 0.062 respectively [19]. The refractive index of As_2S_3 was measured at a photon energy of 1.5 eV, and that of As_2Se_3 was measured at a photon energy of 1.0 eV. The reversible portion of these changes was 0.015 for As_2S_3 and 0.004 for As_2Se_3. Tanaka measured a reversible refractive index change in As_2S_3 of 0.029 at a wavelength of 633 nm [34]. In 2001, we measured refractive index changes as large as 0.05 in thermally evaporated As_2Se_3 thin films [35].

Tanaka measured both the reversible and irreversible refractive index changes for different concentrations of As_xS_{100-x}, and found that the total maximum modulations occurred at $x = 40$, but the reversible changes increased slightly with $x > 40$[36].

It has also been observed that evaporating at different angles of incidence can influence the amount of photodarkening observed in a film. Dikova et al. observed that refractive index changes due to 488 nm illumination in As_2S_3 films were maximized when the film was evaporated at an oblique angle of 70°[37]. The difference between the obliquely deposited film and the normal deposited film was $\Delta n \sim 0.04$. Annealing was not studied in that case.

2.7.2. Photoluminescence (PL)

When light is absorbed in a material and electron - hole pairs are created, they may recombine either radiatively or non-radiatively. Radiative recombination emits light of a different wavelength than the exciting light. Photoluminescence experiments of this kind provide information about the defect structures in a glass. Generally, the chalcogenide glass peak photoluminescence energy is located at about half the band-gap energy for the given glass. In 1973, Street et al. observed that the photoluminescence intensity of chalcogenide glasses decreases after the sample is irradiated with above band-gap light [38]. This result is referred to as photoluminescence fatigue, and is dependant on several factors including irradiation intensity and excitation energy. This fatigue is stable at low temperatures, but is removed by annealing [39]. In 1989, a new low energy PL peak was found at 0.85 eV in a-As_2S_3 after band-gap light illumination [40]. This lower energy peak is excited with sub-band-gap light (1.58 eV), as opposed to the higher peak at 1.1 eV which is excited with near band-gap light (2.41 eV).

2.7.3. Photoconductivity

Chalcogenide glasses are like other semiconductors when illuminated with band-gap light. The light induces the creation of electron – hole pairs which create a current, known as a photocurrent, given a potential difference across the glass. In 1986, it was observed that this photocurrent decreased in value over time as the glass remained illuminated [41]. This current returns to its original dark current when the illuminiation source is turned off. Further study in 1993 showed that the decrease in photocurrent is greater at higher temperatures up to a maximum at 300 K [42]. Also, the higher the intensity of light illumination, the greater the drop in photocurrent. Similar experimental results were obtained for several chalcogenide glasses, including As_2S_3 and As_2Se_3.

2.7.4. AC conductivity

In 1976, Lyubin et al. reported that a-As-Se films exposed to band-gap illumination displayed a 15% increase in its capacitance (imaginary part of ac conductivity) [43]. This effect was removable with annealing at 170 °C. In 1988, Shimakawa showed that for As_2Se_3 films, the real part of ac conductivity also displays an increase after illumination [44]. It was also removable through the annealing process.

2.7.5. Anisotropy

When illuminated with linearly polarized light, linear dichroism ($\alpha_{||} - \alpha_{\perp}$) and linear birefringence ($n_{||} - n_{\perp}$) appear in chalcogenide glass films [45]. Here the subscripts $||$ and $\perp$ refer respectively to the coefficients parallel and perpenducular to the plane of polarization of the exciting radiation. Both the photoinduced dichroism and the photoinduced birefringence can both be removed by either annealing or illuminating with circularly polarized light. In 1989, Lyubin et al. observed that the photoinduced dichroism was annealed out at a much lower temperature than the photodarkening [46]. They concluded that the mechanisms responsible for photoinduced anisotropy are not the same as those responsible for photodarkening.

2.7.6. Oscillator behavior

Using thick films (6μm) of a-$GeSe_2$ evaporated on silica glass substrates, Hajto et al. observed an oscillatory nature in the transmission of below band-gap light [47]. This is shown in Figure 2.11. The glass with band-gap energy of 2.15 eV was illuminated with high intensity (2 kW/cm^2) He-Ne (photon energy = 1.96 eV) light. The intensity of the transmitted light was observed to oscillate. First transmission rises slightly as photobleaching occurs in the glass, which is expected. Then the transmission drops rapidly as a darkened state is reached, before the glass appears to return to the original state and the process repeats itself. The intensity of the illumination laser appeared to control the frequency and amplitude of the oscillation. A higher power laser showed an

increase in the transmittance change and a decrease in oscillation frequency. The oscillation only occurred between light intensities of 1.39 kW cm-2 and 2.65 kW cm-2, and was only observable when illuminating at a photon energy of 1.96 eV. Hajto et al. believe that the oscillation of transmittance is due to repetitive crystallization and melting of the glass.

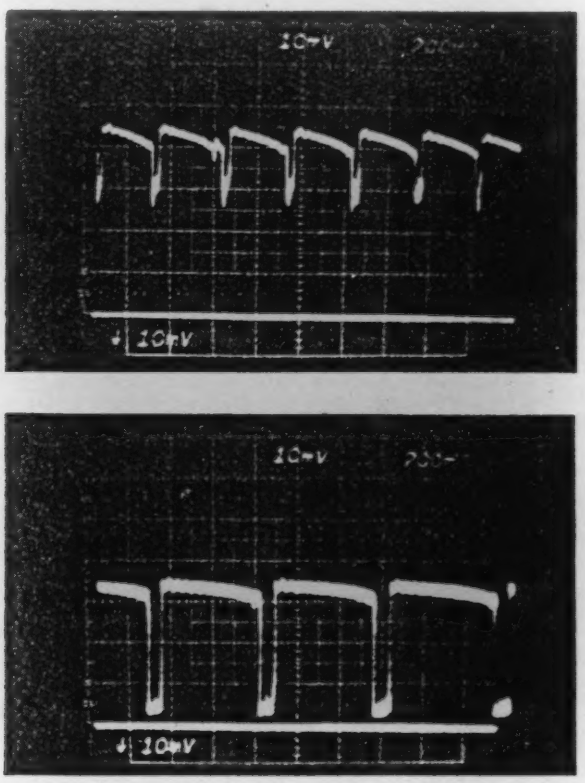

Figure 2.11. Oscillating transmission curves for film of $GeSe_2$. Films were illuminated with a 30 mW Helium-Neon laser with different intensities. Top graph is for illumination intensity of 1.66 kW cm^{-2}, bottom graph is for illumination intensity of 2.6 kW cm^{-2} [47].

2.7.7. Photoamorphization

Elliot and Kolobov observed in 1991 that when a crystallized film of $As_{50}Se_{50}$ on a silica substrate was illuminated with low intensity light the films became amorphous [48]. As

far as they could determine, this phenomenon only appears in films of this composition. Annealing causes a crystalline structure to reform, but it is different from the original.

2.7.8. Photodiffusion (Photodoping)

First observed in 1966 by Kostyshin et al., the diffusion rate of several metals in ChG is increased by illumination [49]. Also observed is that in Ag rich films, under low intensity above band-gap light, Ag has been separated from the glass at the surface [50].

2.7.9. Volume change

Illumination with band-gap light induces an increase in the volume of several chalcogenide glasses, which has been described as photoexpansion. Hamanaka et al. first observed this phenomena [51]. Thin films of annealed As_2S_3 were exposed to a xenon lamp through an infrared filter, and displayed volume changes of around 0.4 %. When heated to 170 °C the volume changes were removed. Expansion was repeatable under subsequent illumination. When the incident laser beam is focused, a greater volume change has been observed and called giant photoexpansion [52]. As_2S_3 flakes displayed volume changes up to 2 % when illuminated with a He-Ne laser source (1.96eV). This illumination source is actually below the band-gap of As_2S_3 (2.34 eV), but is in the Urbach region. Thickness changes in that case were also reversible by annealing. 2.41 eV laser light has also been used to create photoexpansion in As_2S_3 glass, and thickness changes as large as 10% were recorded [53]. Photocontraction has also been reported in $As_4Se_5Ge_1$ by Hamanaka et al. [51], and also for GeS_2 and $GeSe_2$ [26]. The degree of contraction was increased in films that were evaporated at oblique angles. The same was reported for P_4Se_{10} thin films [54]. The columnar structure of these films is thought to play a role in their contraction.

2.8. Gratings

Gratings are fundamental to several photonic devices, and as such have been widely investigated. This sub-section contains a brief report of significant papers on chalcogenide grating research. In 1970, Brandes et al. conducted the first grating experiments in chalcogenide glass [55]. As-S and As-S-Br glasses were studied by illuminating with an interference pattern from a 488 nm laser. Diffraction efficiencies were measured, and it was concluded that the gratings were due to refractive index modulations. However, no values were reported for the induced index change. In 1977, Andriesh et. al. created holographic gratings in thin films of evaporated As_2S_3 [56]. A Helium – Cadmium laser (441.6nm) was the illumination source, and refractive index modulations of 0.02 were reported. In 1981, an argon-ion laser source was used by Yaji et al. to induce gratings in an As_2S_3 thin film [57]. In 1984, gratings in As_2S_3 films were created by silver photodoping [58]. In 1994, melt-quenched As_2S_3 samples were exposed to an ultrahigh pressure Hg lamp through an interference filter to produce a grating [59].

In 1995, gratings were produced in chalcogenide glass fibers for the first time [60]. The optical fibers were made from As_2S_3. A Helium-neon laser (633nm) was coupled into one end of the fiber, and the interference fringes formed by the forward beam and the reflected beam from the exit surface were considered responsible for the induced grating. There was a dip in the transmission spectra at the illuminated wavelength confirming the presence of the grating. Δn was calculated to be 0.002 in the illuminated fibers. In 1996, a transverse holographic method was used to induce gratings in As_2S_3 based fiber [61]. They also used a He-Ne laser to illuminate the fiber, and calculated their Δn of the gratings to be of the order 10^{-4}.

In 1997, volume gratings were created in evaporated As_2S_3 thin films using a transverse holographic method [62]. The illumination source was an argon laser (488 nm). Gratings with periods of 45 μm were measured to have trough to peak volume measurements of 6 nm. In 1999, gratings were created in a multilayer ($As_{24}S_{38}Se_{38}/As_2S_3$) waveguide via a transverse holographic method [63]. The

illumination source was an argon ion laser (514.5nm). Gratings with periods of 353 nm were calculated to have refractive index modulations of around 3×10^{-4}. They also noted that the gratings appeared to be stable at room temperature. Viens et al. (1999) compared the photosensitivies of $As_{24}S_{38}Se_{38}$ and As_2S_3 at different wavelengths of light by writing gratings using both 514 nm and 633 nm sources [15]. At 514 nm, both alloys exhibited photodarkened gratings, with the As_2S_3 gratings being stronger. At 633 nm illumination, the As_2S_3 grating appears to be non-existent, but a weak grating existed in the $As_{24}S_{38}Se_{38}$. The refractive index modulation of As_2S_3 gratings has been difficult to measure, due to the volume modulation that accompanies it. In 2002, Fischer et al. reported that they separated the contribution of these gratings [64]. The gratings were illuminated with an argon ion laser (514 nm), and the refractive index modulation recorded for 1 μm gratings was around 5×10^{-2}.

We have reported gratings in As_2Se_3 thin films with refractive index modulations as large as 0.037 [65,66].

2.9. Summary

This chapter gave a brief review of the investigation of chalcogenide glasses over the last few decades. The effects that can be photoinduced by near band-gap light are numerous, and are still only partially understood. All of the effects appear to be wavelength dependant, alloy-dependant, temperature-dependant, as well as dependant on the glass preparation method. Each series of glasses and effects are potentially of technological interest. The potential applications of ChG are numerous and include gratings, micro-lenses, amplifiers, optical switches, and waveguides.

This thesis is a study of As_2Se_3 thin films for the fabrication of sub-micron gratings, using a standard He-Ne laser source.

Chapter 3

Holographically Induced Bragg Gratings: Theory and Experimental Setup

3.1. Theory of holographically induced gratings

Bragg gratings are used as wavelength selective mirrors in several photonic devices, including filters, semiconductor lasers, and multiplexors. Because of their dispersive properties, they also are used for soliton generation and dispersion compensation in optical communication systems. The top view of a Bragg grating is shown in Figure 3.1, as it would be used in a waveguide. The grating consists of a periodic variation in either the structure of the waveguide or the refractive index of the waveguide. When several wavelengths of light propagate in a waveguide that contains such a grating, the wavelengths that satisfy the Bragg condition (λ_B) are reflected back, while other wavelengths are transmitted through. The Bragg condition is,

$$m\lambda_B = 2n_{eff}\Lambda \qquad (3.1)$$

where m is the order of the grating, n_{eff} is the effective refractive index of the waveguide, and Λ is the period of the grating.

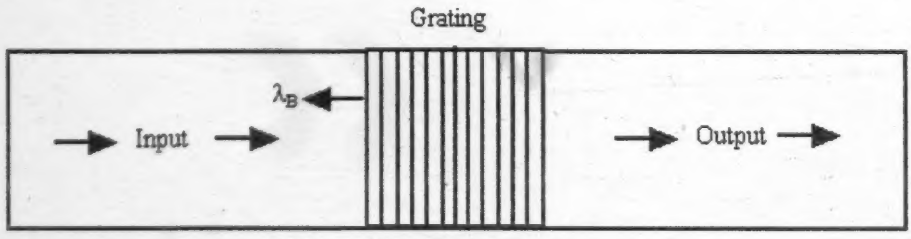

Figure 3.1. Top view of a Bragg grating, as used in a waveguide structure. Communication data on multiple wavelength carriers propagate from left to right, but at the grating the Bragg wavelength is reflected and will not be part of the output data.

As mentioned in the previous chapter, chalcogenide glass is sensitive to band-gap light. Appropriate illumination causes a shift in its absorption edge, which is accompanied by a

change in the refractive index of the glass. If a periodic variation in illumination intensity (such as created by interfering two coherent laser beams) is used, a refractive index-based Bragg grating can be created. By interfering two coherent laser beams as shown in Figure 3.2, a spatially modulated field is produced, with a period determined by the angle between the beams.

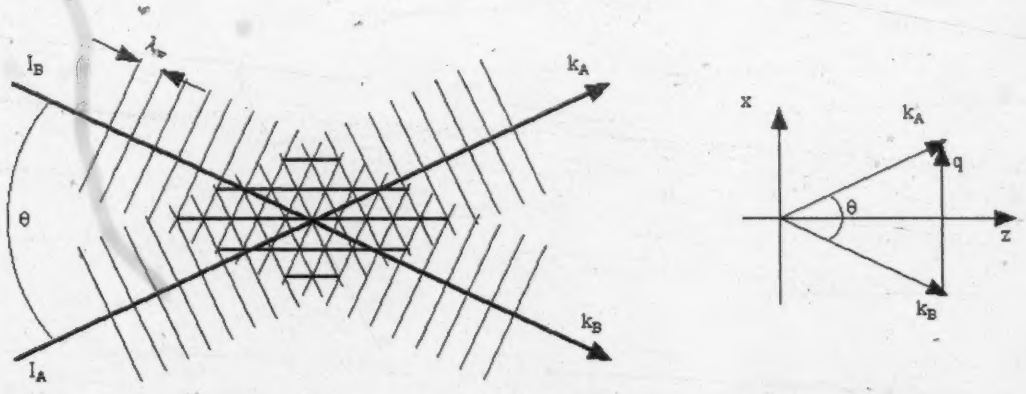

Figure 3.2. An interference pattern created by two coherent light beams can be used in light sensitive materials to induce gratings. The writing beams have intensities I_A and I_B, wavevectors k_A and k_B, wavelengths λ_w and interfere at an angle θ. The resulting grating has a grating vector, q.

In practice, light from a single laser is split into two beams A and B, with wave vectors $\mathbf{k}_A$ and $\mathbf{k}_B$, electric field amplitudes $\mathbf{A}_A$ and $\mathbf{A}_B$, and intensities I_A and I_B. The intersection angle of the two beams at the sample is θ. This produces an interference pattern corresponding to a grating vector **q**,

$$\mathbf{q} = \mathbf{k}_A - \mathbf{k}_B = (2\pi/\Lambda)\cdot\mathbf{x}\,. \tag{3.1}$$

Λ is the period of the grating, and **x** is the unit vector in the x-direction. The wavevectors $\mathbf{k}_A$ and $\mathbf{k}_B$ can be written with respect to the Cartesian coordinates k_x and k_z, since it is assumed they are in the x-z plane.

$$\mathbf{k}_A = k_z\,\mathbf{z} + k_x\,\mathbf{x}\ , \tag{3.2a}$$

$$\mathbf{k}_B = k_z\,\mathbf{z} - k_x\,\mathbf{x}\ , \tag{3.2b}$$

where **x** and **z** are the respective unit vectors. Plane-wave beams are assumed, so that variation in the y-direction is neglected.

Note also that

$$k_x = k_A \sin(\theta/2)\ , \tag{3.3a}$$

$$k_z = k_A \cos(\theta/2) \ . \qquad (3.3b)$$

We can rewrite the grating vector and scalar as,

$$\mathbf{q} = \mathbf{k_A} - \mathbf{k_B} = 2k_x\mathbf{x}, \qquad q = 2\frac{2\pi}{\lambda_w}\sin\left(\frac{\theta}{2}\right). \qquad (3.4)$$

Comparing equation (3.1) and (3.4) we can show that the period of the grating is given by the equation,

$$\Lambda = 2\pi/q = \frac{\lambda_w}{2\sin(\theta/2)}, \qquad (3.5)$$

where λ_w is the wavelength of the writing beam. The period of the grating can be altered by either changing the wavelength of the writing laser or by changing the angle of incidence, θ. Equation (3.5) sets a minimum limit for the period of the grating, which occurs when $\sin(\theta/2) = 1$. This occurs when the two beams interfere at an angle of 180 degrees. The period of the grating in this case is half the writing wavelength.

The electric field in the interference region is the superposition of the two writing beams,

$$\mathbf{E} = \frac{\mathbf{A}}{2} e^{i(k_z z - \omega_w t)} + \text{c.c.} \ , \qquad (3.6)$$

where the amplitude is,

$$\mathbf{A} = \mathbf{A_A}\, e^{ik_x \mathbf{x}} + \mathbf{A_B}\, e^{-ik_x \mathbf{x}} \ . \qquad (3.7)$$

Assuming equal intensity beams, both polarized along the same direction, the intensity distribution in the plane of the sample is

$$I(x) = \frac{n}{2}\varepsilon_o c(A \bullet A^*) = 2I_A + 2I_A \cos(qx) \qquad (3.8)$$

The intensity thus varies between zero and four times the intensity of a single beam, periodically along the x-direction.

The above theory describes the basic experimental setup used to photoinduce gratings in silica glass fibers, which are of great commercial importance. The same technique was used in this work to photoinduce gratings in chalcogenide glass thin films. Chalcogenide glasses are light sensitive and undergo changes to both the refractive index and the absorption coefficient. The complex refractive index can be written as

$$\tilde{n} = n + i\ \alpha/2k\ , \tag{3.9}$$

where n is the real part of the refractive index, α is the absorption coefficient, and k is the wave number.

3.2 Characterization of Bragg gratings using diffracted beams

Some gratings can be detected by transmitting a probe beam through the grating as shown in Figure 3.3(a), and measuring the diffracted waves. Each diffracted beam is at an angle Φ_m, where

$$\sin\Phi_m = m\lambda_p/\Lambda\ ,\ m = 0, \pm1, \pm2, \ldots \tag{3.10}$$

The smallest grating period that can be detected in this manner is for $\sin\Phi = 1$, and corresponds to a grating with a period equal to the probe wavelength.

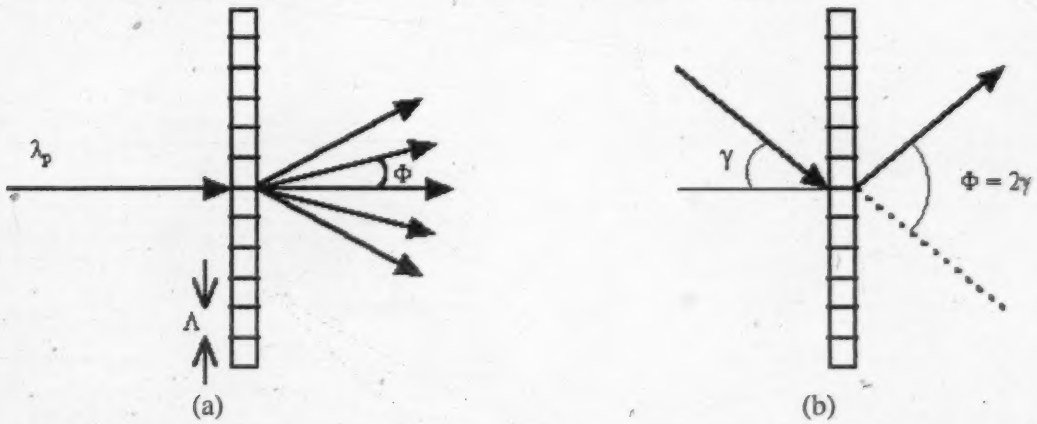

Figure 3.3. Gratings can be detected by transmitting a probe beam (a) perpendicular to the glass surface or (b) at its Bragg angle. The probe beam is diffracted at the angles Φ.

An alternate method of detection is to angle the probe beam as shown in Figure 3.3(b). For sufficiently thick gratings, coupled - wave theory can be used to analyze such gratings [67]. If the light incident on the hologram grating is at, or near the Bragg angle and polarized perpendicular to the plane of incidence, only two beams need to be considered: the incoming incident wave, and the outgoing first order diffracted wave. These are the only two waves that satisfy the Bragg condition. All the other diffraction orders violate the Bragg condition and are neglected, as they should not influence the interchange of energy between the incident and first order diffracted waves.

The permitivity ε is assumed to be spatially modulated,

$$\varepsilon = \varepsilon_0 + \varepsilon_1 \cos(q \bullet x), \tag{3.11}$$

and is related to the refractive index and absorption coefficient by the equation,

$$\varepsilon = (\tilde{n})^2 = n^2 + in\alpha / k - \alpha^2 / 4k . \tag{3.12}$$

The incident wave is given by

$$A_i = \frac{A_i}{2}\exp(k_i r) + c.c. = \frac{A_i}{2}\exp(k_i r)\left[ik_i(x\sin\gamma + z\cos\gamma)\right], \tag{3.13}$$

where γ is the angle of incidence measured inside the material.

Wave propagation in the grating is described by the scalar wave equation

$$\nabla^2 E + k^2 \varepsilon E = 0 . \tag{3.14}$$

The field inside the grating is expressed as a superposition of plane waves with amplitudes S_m varying in the z- direction

$$E(x,z) = \sum_m S_m(z)\exp(i\sigma_m r) , \tag{3.15}$$

where σ_m are the wavevectors inside the gratings:

$$\sigma_m = \text{ki-mq, m} = 0, \pm 1, \pm 2, \tag{3.16}$$

Substituting (3.11, 3.15) into (3.14), and performing the differentiations gives

$$\sum_m \left[\begin{array}{l} \dfrac{\partial^2 S_m}{\partial z^2} + 2i\left(k_i \cos\gamma - mq\cos\phi\right)\dfrac{\partial S_m}{\partial z} - \sigma_m \bullet \sigma_m S_m \\ +k^2 \varepsilon S_m + \dfrac{k^2 \varepsilon_1}{2} S_{m-1} + \dfrac{k^2 \varepsilon_1}{2} S_{m+1} \end{array} \right] \exp(i\sigma_m \bullet r) = 0 \tag{3.17}$$

This equation must be satisfied for all the variables, and the coefficients of each exponential must be equal to zero. Note also that $k_i = nk$, and $k = 2\pi/\lambda$, so that the following coupled wave equation is obtained.

$$\frac{\partial^2 S_m}{\partial z^2} + 4\pi i\left(\frac{n\cos\gamma}{\lambda} - \frac{m\cos\phi}{\Lambda}\right)\frac{\partial S_m}{\partial z} + \frac{4\pi^2 m}{\Lambda^2}\left[\frac{2n\Lambda}{\lambda}\cos(\gamma-\phi) - m\right]S_m + \frac{4\pi^2}{\lambda^2}\left(\varepsilon - n^2\right)S_m + \frac{2\pi^2\varepsilon_1}{\lambda^2}\left(S_{m-1} + S_{m+1}\right) = 0 \tag{3.18}$$

When certain approximations are made, simplifications are possible, and the normally rigorous solution becomes less complex. If the partial wave amplitudes, $S_m(z)$, vary slowly over distances comparable to the wavelength, then the second derivatives may be neglected. It is also assumed that the absorption is small ($\varepsilon - n^2 \approx in\alpha/k$), and that the gratings are unslanted ($\phi = \pi/2$). When the Bragg condition is met for the first-order diffracted wave, all terms but S_0 and S_1 may be neglected, and the partially differential equations of (3.18) become,

$$\frac{dS_0}{dz} = -\frac{\alpha}{2\cos\gamma}S_0 + i\frac{\pi\varepsilon_1}{2n\lambda\cos\gamma}S_1$$
$$\frac{dS_1}{dz} = -\frac{\alpha}{2\cos\gamma}S_1 + i\frac{\pi\varepsilon_1}{2n\lambda\cos\gamma}S_0 \tag{3.19}$$

The solution to these equations, with the initial conditions $S_0(z = 0) = A_i$ and $S_1(z = 0) = 0$ is,

$$S_0 = A_i\exp\left(-\frac{\alpha z}{2\cos\gamma}\right)\cos\left(\frac{\pi\varepsilon_1 z}{2n\lambda\cos\gamma}\right)$$
$$S_1 = iA_i\exp\left(-\frac{\alpha z}{2\cos\gamma}\right)\sin\left(\frac{\pi\varepsilon_1 z}{2n\lambda\cos\gamma}\right) \tag{3.20}$$

Where,

$$\sqrt{\varepsilon} = \tilde{n} = n + i\alpha\lambda/4\pi$$
$$\varepsilon_1 = \Delta\varepsilon \approx 2\tilde{n}\Delta\tilde{n} \approx 2n\left(\Delta n + i\lambda\Delta\alpha/4\pi\right) \tag{3.21}$$

For mixed gratings consisting of changes to both the refractive index and absorption, the transmitted I_0 and I_1 intensities, normalized to the incident intensity I_i are given by the following two equations:

$$\frac{I_0}{I_i} = \exp\left(\frac{-\alpha z}{\cos\gamma}\right)\left[\cos^2\left(\frac{\pi\Delta n z}{\lambda\cos\gamma}\right) + \cosh^2\left(\frac{\Delta\alpha z}{4\cos\gamma}\right) - 1\right] \tag{3.22}$$

$$\frac{I_1}{I_i} = \exp\left(\frac{-\alpha z}{\cos\gamma}\right)\left[\sin^2\left(\frac{\pi\Delta n z}{\lambda\cos\gamma}\right) + \sinh^2\left(\frac{\Delta\alpha z}{4\cos\gamma}\right)\right] \tag{3.23}$$

At the probe wavelength, where the glass is highly transmissive, we assume that the absorption-based terms of equations (3.22) and (3.23) are negligible compared to the refractive index-based terms. By dividing equation (3.23) by (3.22) and neglecting the contribution from the absorption change, a simple expression for the diffraction efficiency is formed.

$$\eta = \frac{I_1}{I_0} = \tan^2\left(\frac{\pi\Delta n z}{\lambda\cos\gamma}\right) \tag{3.24}$$

This assumption is justified with experimental data in Chapter 4.

By measuring the diffraction efficiency of the grating, and using equation (3.24), the refractive index modulation of the grating, Δn, can be determined.

3.3 Grating writing experiment

The experimental setup for writing and simultaneously detecting the photoinduced refractive index based gratings is shown in Figure 3.4 and Figure 3.5. The equipment used is listed in Appendix A.

The writing laser was a 10 mW Helium Neon source with wavelength 632.7 nm. An electronic shutter was used to precisely control the writing time. A linear polarizer (LP) was used to ensure the light was polarized perpendicular to the plane of incidence. Two lenses (L1 and L2) were used to expand the beamwidth. A 50/50 beam splitter (BS) then splits the writing beam into two paths where mirrors (M1 and M2) redirect the beams onto the surface of the Chalcogenide glass (ChG) sample. Each beam at the ChG sample was measured to have a power of 4.8 mW, and the beam diameter of around 4 mm. The angle these beams make with the perpendicular of the glass is given by the angle θ. Cleaned microscope slides are used as the substrate for the As_2Se_3 thin films. This allows

transmissive probing to monitor the strength of the gratings during the writing process (see Chapter 4). The probe laser is also shown in the diagram. The laser used for this purpose was an 839 nm laser, with a power of 1 mW, and a beam diameter of 1.5 mm. The angle the probe beam makes with the perpendicular to the glass surface is γ. Two infrared photodetectors (PD1 and PD2) are used to measure the transmitted and diffracted beam powers (zeroth and first order diffraction). These powers were recorded with a computer and the diffraction efficiency was monitored in real time. The results of such measurements are discussed in Chapter 4.

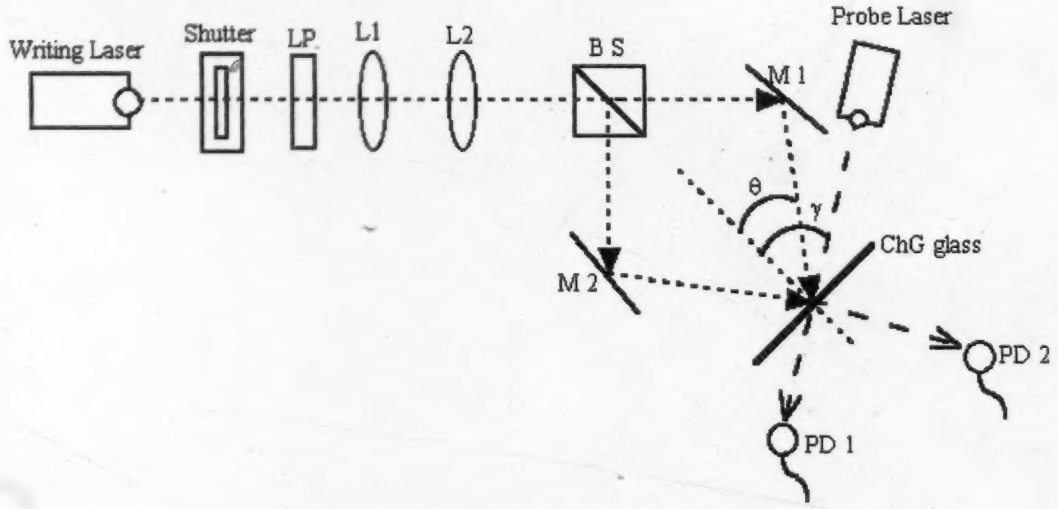

Figure 3.4. Setup to write and probe Bragg gratings on Chalcogenide glass thin films.

The probe laser with an 839 nm wavelength was chosen because it is well below the band-gap of As_2Se_3. The gratings were designed for eventual use in waveguides operating at 1550 nm. The Bragg condition was given in equation (3.1), and is rewritten here.

$$m\lambda_B = 2n_{eff}\Lambda \qquad (3.1)$$

λ_B is the Bragg wavelength reflected, n_{eff} is the refractive index of the waveguide, and Λ is the period of the grating. Assuming $n_{eff} \approx 2.73$ for an As_2Se_3 – based waveguide, the first order Bragg grating (m = 1) has a period of 285 nm, and the second order Bragg grating (m = 2) has a period of 570 nm. The grating induced by the setup in Figure 3.4 has a period given by equation (3.25).

$$\Lambda = \lambda_w/2\sin(\theta)\,. \qquad (3.25)$$

Here λ_w is the writing laser wavelength, and θ is the angle each incident beam makes with the perpendicular to the glass. The minimum period that can be induced by this setup is equal to $\lambda_w/2$, which for 633 nm light is 316.5 nm. Therefore it is not possible to write first order Bragg gratings of period 285 nm, and second order gratings were targeted. Equation (4.1) implies $\theta = 33.7°$ for 570 nm gratings. Measurements showed that the as-written grating periods were closer to 560 nm.

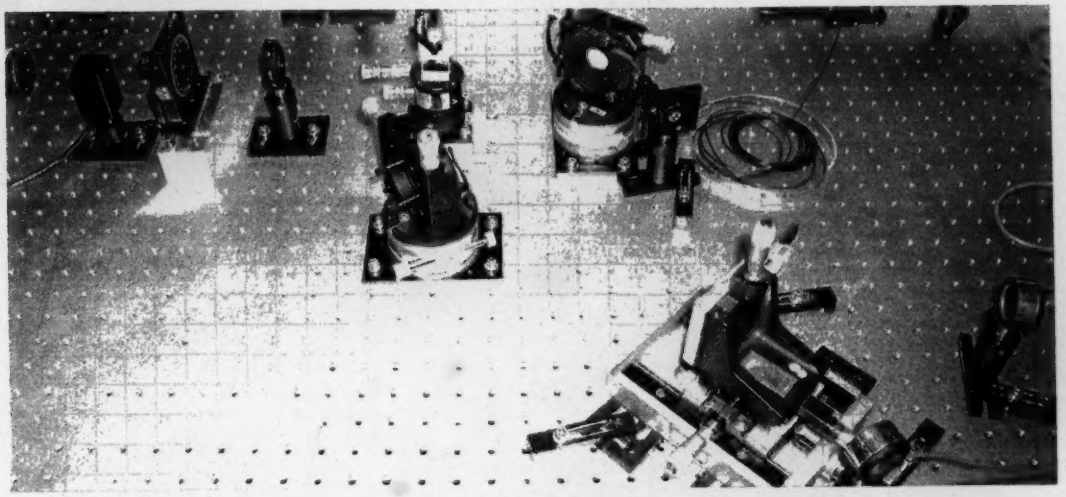

Figure 3.5. Photograph of setup to write and probe Bragg gratings on Chalcogenide glass thin films.

The probe beam, as explained in chapter 3, must be at or near its Bragg angle for our analysis to hold. Its angle is given by the following equation,

$$\sin\gamma = \lambda_{probe}/2n\Lambda\,, \qquad (3.26)$$

where λ_{probe} is the probe wavelength (839 nm), γ is the angle of the probe beam inside the glass, Λ is the period of the grating (560 nm), and n is the average refractive index of the glass in the grating region for the probe wavelength (n = 2.87 @ 839 nm). Equation (3.26) yields $\gamma = 15.1$. The angle outside the glass is 48.4°, according to Snells law.

3.4. As_2Se_3 Chalcogenide Glass Samples

Table 2.1 listed several chalcogenide glasses along with their band-gaps, and each of them has potential application to integrated optics. As_2Se_3 was chosen for study here, owing to several interesting properties. Photodarkening in As_2Se_3 has received less attention than photoinduced processes in certain other ChG alloys (especially As_2S_3), in spite of the fact that it is a convenient glass to study. It is a commercially available alloy that can be thermally evaporated to form high quality thin films. Further, it has a band-gap of 1.76 eV, and is efficiently photodarkened using standard HeNe lasers (E_{photon} =1.96 eV). As_2Se_3 is also one of the most promising glasses for all-optical switching and signal processing at 1550 nm wavelength, with a Kerr coefficient that is ~ 1000x that of silica glass [10].

The a-As_2Se_3 samples used in the work were thermally evaporated onto room temperature substrates. The thicknesses of the films varied from 1 μm to 3 μm, and the films were not annealed after deposition. The substrates used were cleaned common microscope slides. The prepared samples were obtained from the University of Saskatchewan (Dr. S. O. Kasap). Figure 3.6 is a photograph of one As_2Se_3 glass sample under illumination.

Figure 3.6. Photograph of As_2Se_3 glass sample in a holder being illuminated with He-Ne laser.

Chapter 4

Results and Discussion

4.1. Diffraction efficiency measurements

A simple measurement of diffraction efficiency is given by equation (3.24), repeated as Equation (4.1),

$$\eta = \frac{I_1}{I_0} = \tan^2\left(\frac{\pi \Delta n z}{\lambda \cos\gamma}\right). \qquad (4.1)$$

I_0 and I_1 are the transmitted and first order diffracted probe beam respectively, γ is the probe angle inside the glass, z is the thickness of the glass, and Δn is the refractive index modulation.

The experimental setup was discussed in the previous chapter. Precision and stability were found to be critical to the experiment. Also, every time the period of the grating was to be changed, realignment was required. Figure 4.1 is an optical microscope photograph of a grating that was induced in an a-As_2Se_3 thin film. The grating is visible due to the photodarkening that accompanies the index change. The microscope was used in transmission mode (with illumination from underneath the sample) allowing us to observe the photodarkened grating. The period of the grating shown in Figure 4.1 is 0.56 μm.

Alignment to induce gratings was quite laborious, but probing the magnitude of the gratings was found to be even more so. The probe beam must be transmitted through the glass at the center of the grating for precision, and it must be very close to the Bragg angle of the grating. Initially, this required several trials, measuring for maximum diffraction. Once alignment was achieved, the diffraction efficiency was recorded in real- time, as the grating was being photoinduced. Figure 4.2 displays a series of

diffraction efficiency measurements at different locations on the same chalcogenide glass sample. The intensity of each arm of the interferometer was ≈ 0.382 mW/mm^2.

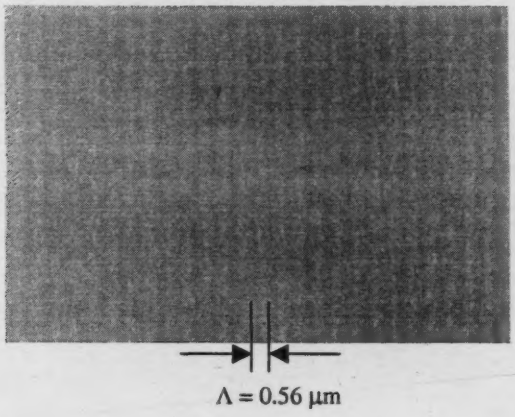

Figure 4.1. Microscopic photograph of a grating photoinduced in a-As_2Se_3 thin film.

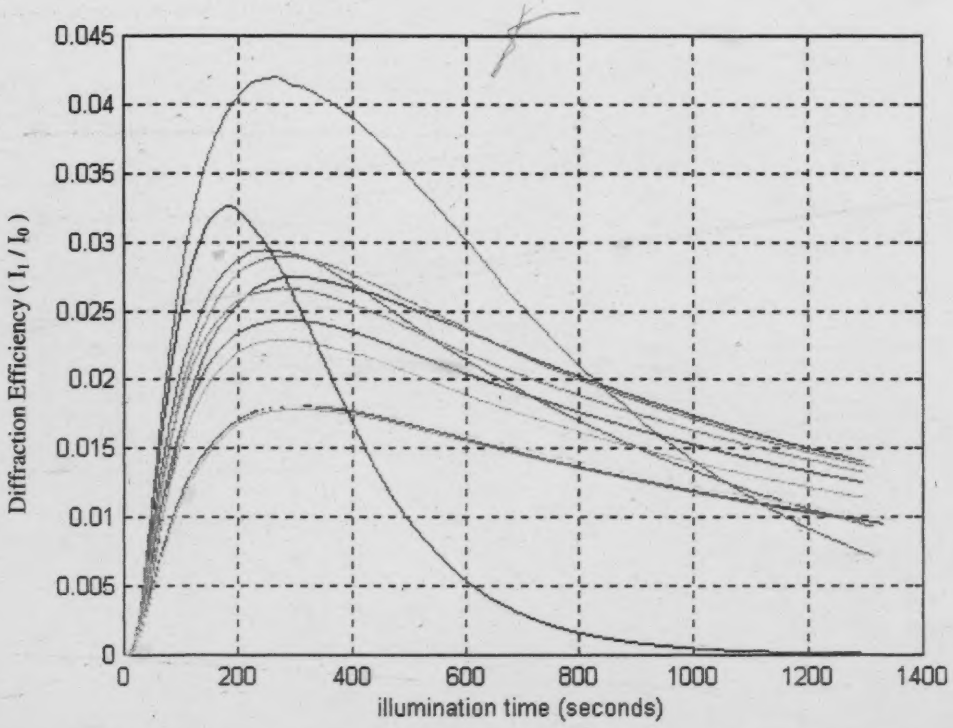

Figure 4.2. Diffraction efficiency plotted in real time during illumination, for several gratings written at different locations on a single As_2Se_3 sample.

Two of the lines in the plot appear anomalous and were omitted from Figure 4.3. The justification for this is discussed in Section 4.4.

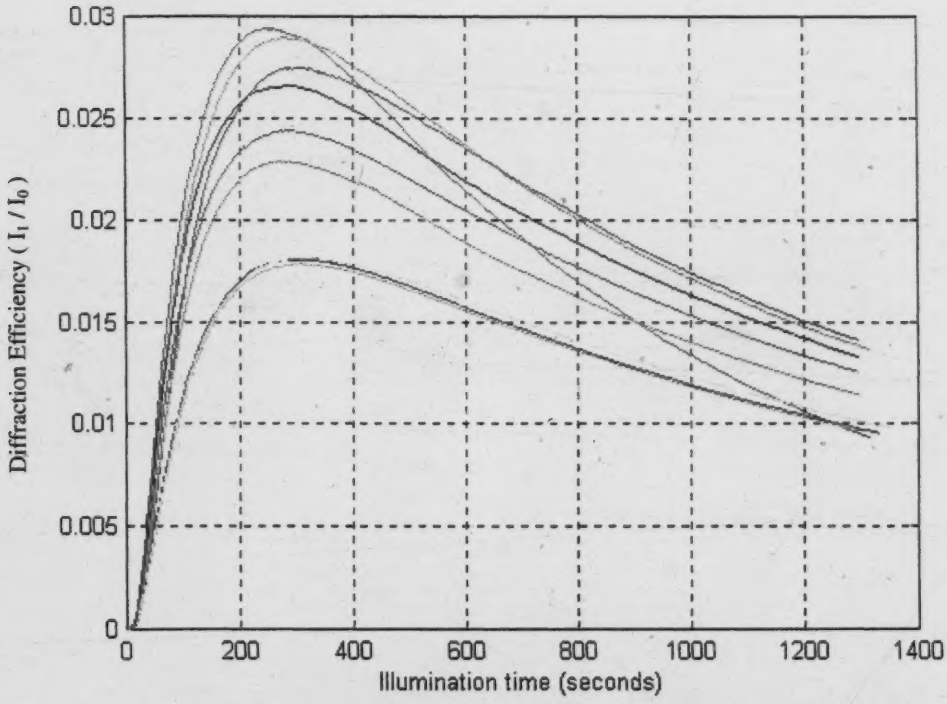

Figure 4.3. Diffraction efficiency plots probed during illumination at various locations on the same a-As_2Se_3 thin film sample. Film thickness varied from 1.18 μm to 1.21 μm, as determined by profilometer measurements. The intensity in each arm was = 0.382 mW/mm^2.

All of the diffraction efficiency plots in Figure 4.3 follow very similar traces. They increase rapidly to a peak located at a characteristic illumination time (around 250 seconds), then slowly decrease. The peak efficiencies shown range between 1.78% and 2.94%.

The scatter in the results was attributed to poor film quality for the ChG samples used in these early experiments. Surface aberrations were clearly visible, and thickness varied significantly over the surface of the film. These factors influence the grating diffraction efficiencies, which therefore depends on the particular location on the sample.

We can create plots of Δn, by extracting it from the measured diffraction efficiency values using equation (3.24).

$$\Delta n = \operatorname{atan}\left(\sqrt{\eta}\right)\left(\frac{\lambda \cos\gamma}{\pi z}\right) \tag{4.2}$$

The thickness differential across the film was taken into account by individually measuring the film thickness (z) at the location of each individual grating. The thicknesses were measured by removing a portion of the ChG film and using a profilometer. Thicknesses varied from 1.18 μm to 1.21 μm for the trials plotted in Figure 4.3. No correlation was observed between film thickness and Δn. The resulting plots of Δn (Figure 4.4) show less scatter than the diffraction efficiency plots above.

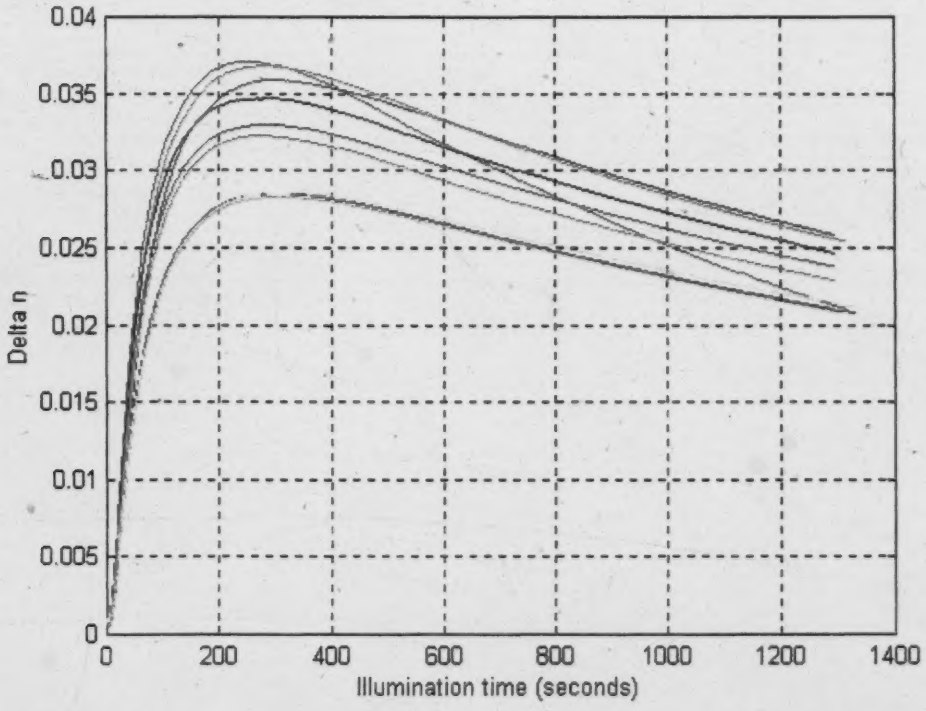

Figure 4.4. Grating Δn versus illumination time for several gratings located on the same a-As_2Se_3 thin film, with the local film thickness taken into account. Film thickness varies from 1.18 μm to 1.21 μm.

The peak value of Δn varies from 0.0285 to 0.0368.

Besides the fact that there is some scatter in the results, it is also clear that there is a reduction in Δn beyond the peak. The obvious question to ask is whether or not the refractive index change starts to decrease after a certain amount of time. From separate uniform illumination experiments, this is not believed to be the case [35]. The decrease in Δn is attributed to the practical realities of the holographic illumination pattern used to produce the gratings. It is not a periodic on/off step-like pattern described in simplified terms in a previous chapter. The pattern itself is in fact a slightly raised sinusoid, where some finite amount of light (energy) is found in the dark portions of the interference pattern. This is due to any slight imbalance in the powers of the two interfering beams, as well as to any vibrational instabilities present in the experiment. This small amount of energy contributes very little in early illumination, but does begin to affect the grating strength once the photodarkening light portions of the pattern begin to saturate.

The same experiment was repeated on a thicker sample, as described in the following paragraphs, and shown in Figure 4.5.

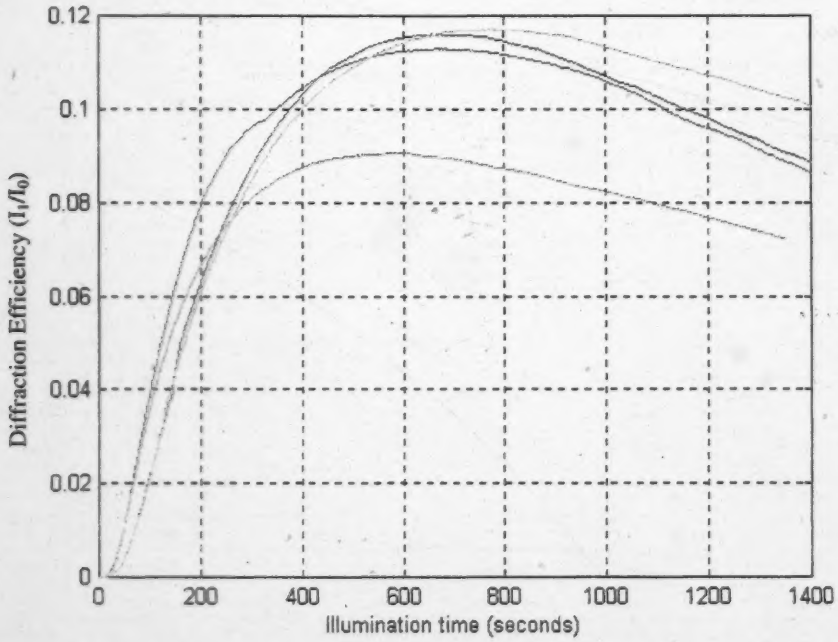

Figure 4.5. Diffraction efficiency plots probed during illumination at various locations on a single a-As_2Se_3 thin film sample. Film thickness varied from 2.10 μm to 2.43 μm.

Also worth noting is that the refractive index of the gratings appear to change more slowly in the thicker sample. Also the maximum Δn is reached after longer illumination. Most peaked at around 700 seconds of illumination, whereas they peaked at around 250 seconds for the thinner sample.

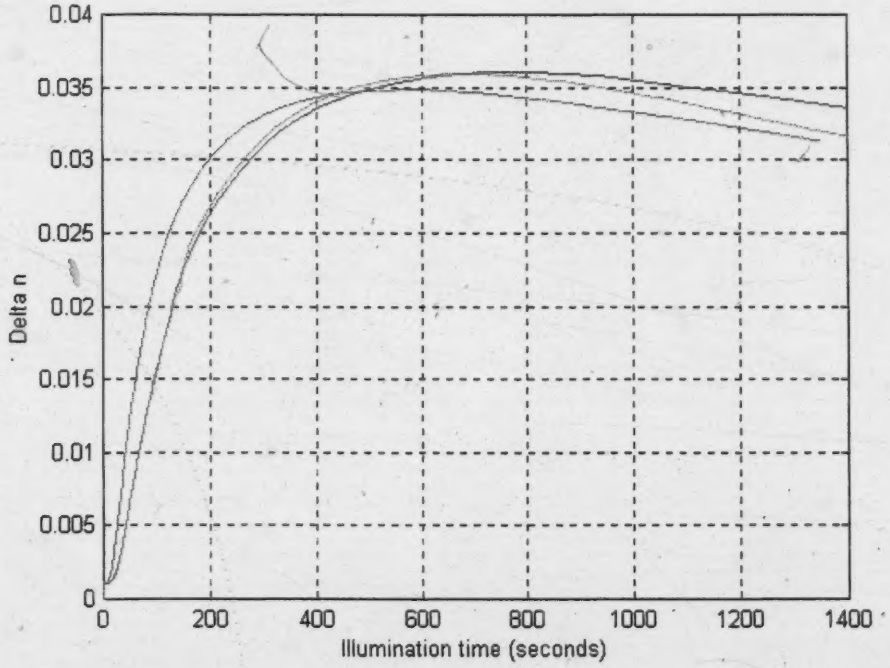

Figure 4.6. Grating Δn versus illumination time for several gratings located on the same a-As_2Se_3 thin film. Film thickness varies from 2.10 μm to 2.43 μm.

4.2. Graphing with respect to energy

Figures 4.4 and 4.6 show how the Δn of the induced gratings varies with illumination time. This, however, does not consider the power or energy of the writing beams. It is illustrative to plot Δn versus the energy used to write the gratings. Figures 4.4 and 4.6 are redrawn here with Δn plotted as a function of dosage. The energy dosage is defined here as the total power of the writing beams multiplied by the writing time and divided by the area of illumination. Using this definition, the plots of Figure 4.4 and 4.6 are re-plotted in Figures 4.7 and 4.8. The intensity of each beam was still ≈ 0.382 mW/mm^2.

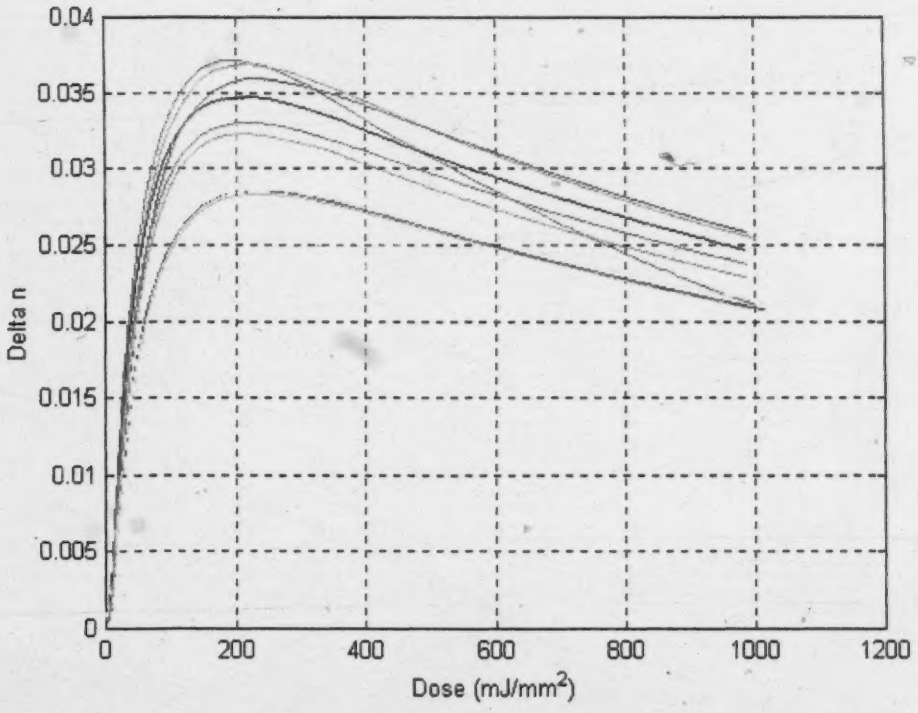

Figure 4.7. Grating Δn versus energy dose for Bragg gratings induced on thin film ranging in thickness from 1.18 μm to 1.21 μm. Peak grating strength occurs in all gratings around an applied energy dose of 225 mJ/mm^2.

Figure 4.7 shows that the first set of gratings reached their maximum strength after a dose of around 225 mJ/mm^2, and Figure 4.8 shows that the second set of gratings reached their maximum quality after a dose closer to 500 mJ/mm^2. The higher energy requirement was probably due to the thicker films in the second case (note that the second film was approximately twice as thick as the first).

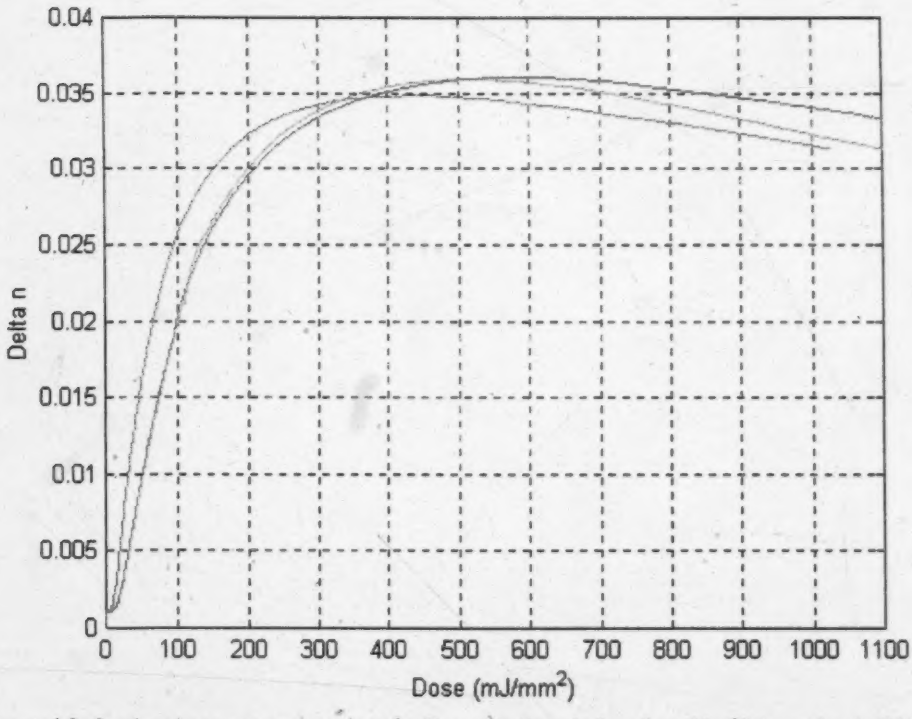

Figure 4.8. Grating Δn versus energy dose for Bragg gratings induced on thin film ranging in thickness from 2.10 μm to 2.43 μm. Peak grating quality occurs in all gratings around an applied energy dose of 500 mJ/mm^2.

4.3. Related experiments

It was noted in Section 2.7.1 that we previously measured refractive index changes in As_2Se_3 as large as 0.05 [35]. The Swanepoel method used for this single beam illumination experiment is described in Appendix B.

At the beginning of this chapter, as well as in Chapter 3, it was mentioned that the minimum period of any holographically induced grating is limited by the wavelength of writing light. From equation (3.25), we see that the minimum period of a grating that can be photoinduced is equivalent to half the wavelength of the writing beam wavelength. With the 633 nm He-Ne laser that was used here, the minimum grating period is 316.5 nm. To photoinduce gratings with smaller periods, a laser with smaller wavelength is

required. An attempt was made to write gratings with a 2 mW yellow (λ = 594 nm) He-Ne laser, as well as a 2 mW green (λ = 544 nm) He-Ne laser. In both cases, gratings were undetectable by the probe beam, but were faintly observable using an optical microscope. These two sources could be used to write gratings with periods as small as 297nm and 272nm, for the yellow and green lasers respectively.

The drawback with using these lasers is the highly absorptive nature of As_2Se_3 glass at these wavelengths. The absorption coefficient of the glass used is shown in Figure 4.9 over the visible to near infrared wavelength range. At 594nm (yellow) the absorption coefficient is around $2x10^6\ m^{-1}$, which means the absorption length is approximately 0.5 μm. Also at the lower wavelength of 544nm (green) the absorption coefficient is around $4x10^6 m^{-1}$, which means the absorption length is approximately 0.25 μm. Therefore the gratings created using these wavelengths of light are limited to the surface of the thin film. This is believed to be one of the reasons that the gratings exposed using the yellow and green sources were difficult to measure.

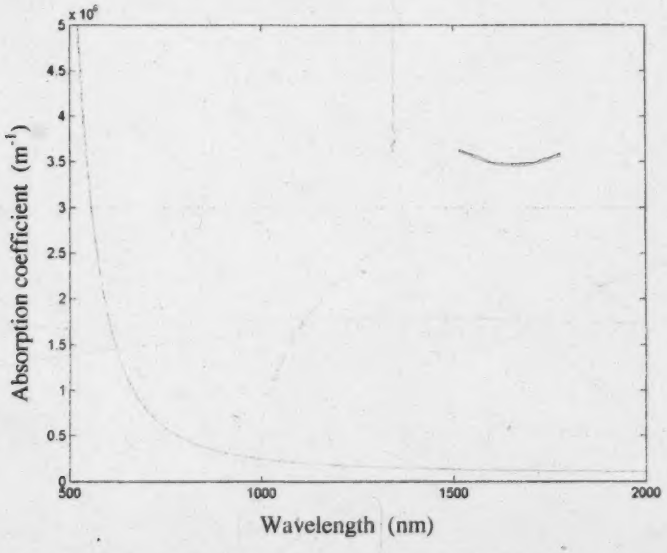

Figure 4.9. Absorption coefficient of As_2Se_3 over the visible to near infrared wavelength range.

4.4. Additional experimental observations and difficulties

Prior to obtaining the results displayed in Figure 4.3, several other trial gratings were induced with less success. It should be noted that the setup of the probe beam is not as simple as one might assume. First, the optical height must be the equal to that of the writing beams. Second, the probe beam must be incident on the glass in the middle of the grating writing area, where the writing beams are most uniform. This is the reason to expand the writing beams via the two lenses shown in Figure 3.4. The writing beam diameters were 4 mm at the glass surface, whereas the probe beam diameter was 1.2 mm. The beam diameter was defined by the $1/e^2$ value of beam power. Thus the beam diameter contains 86.5 % of the total beam power. Another difficulty with the probe beam was due to the fact that it was in the infrared spectrum, and an infrared viewer was required to image the beam. This made setting its incident location and angle quite difficult.

Another problem that was encountered in the experiment was surface imperfections in the chalcogenide glass thin films used. Anomalous diffraction efficiency graphs were occasionally observed even between locations on the same sample. An example is shown in Figure 4.10. We primarily attribute these anomalies to inconsistent surface quality. Any unexpected roughness on the film surface, including dust, will alter the transmission and diffraction of the probe laser beam and thus affect the diffraction measurements.

After some early experiments, it was noted that the two writing beam arms were not of equal power. This caused the quality of the gratings to decrease more rapidly than when the beams were made equal. An example of this is shown in Figure 4.11. The unequal beams had powers of 4.8 mW and 5.3 mW. An attenuator was added to the higher of these two beam arms to make both equal at 4.8 mW.

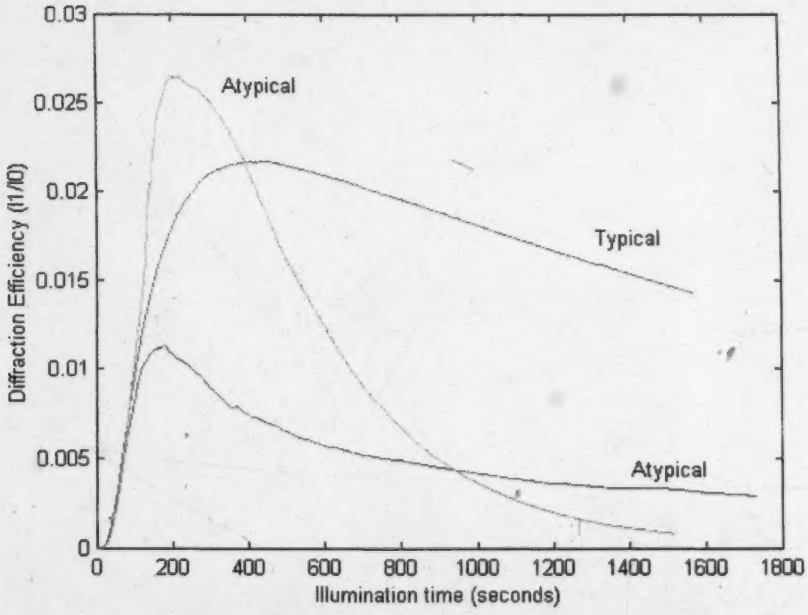

Figure 4.10. Diffraction efficiency graph comparing typical diffraction plot with two atypical plots. The inconsistencies were assumed to be caused by poor surface quality.

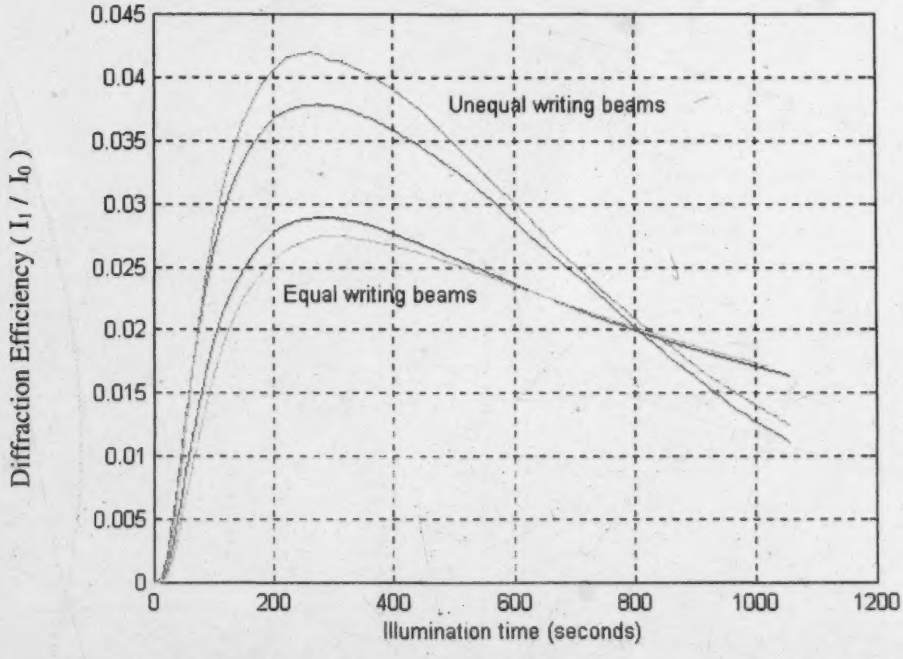

Figure 4.11. Diffraction efficiency graph comparing gratings written with unequal writing beams and those with equal writing beams. Note that the higher peak diffraction efficiency in the first case is attributable to a greater film thickness.

Note that the gratings written with unequal writing beams were on thicker films. The equal beam gratings were induced on thin films of around 1.18 μm thickness, while the unequal beam gratings were induced on thin films of around 1.35 μm. When the gratings of Figure 4.11 are plotted as Δn versus time, the maximum Δn achieved was similar, as shown in Figure 4.12. The reason why there is such a rapid falloff in the diffraction efficiency of gratings induced with unequal beams is due to the interference pattern created with those beams. In Section 4.1, the interference pattern created by the two beams was described to be a raised sinusoid, where some finite energy is found in the troughs of the interference pattern. The energy in these regions is increased when the interfering beams are of different energy. This causes a more severe falloff in the diffraction efficiency of the gratings, as well as the Δn values.

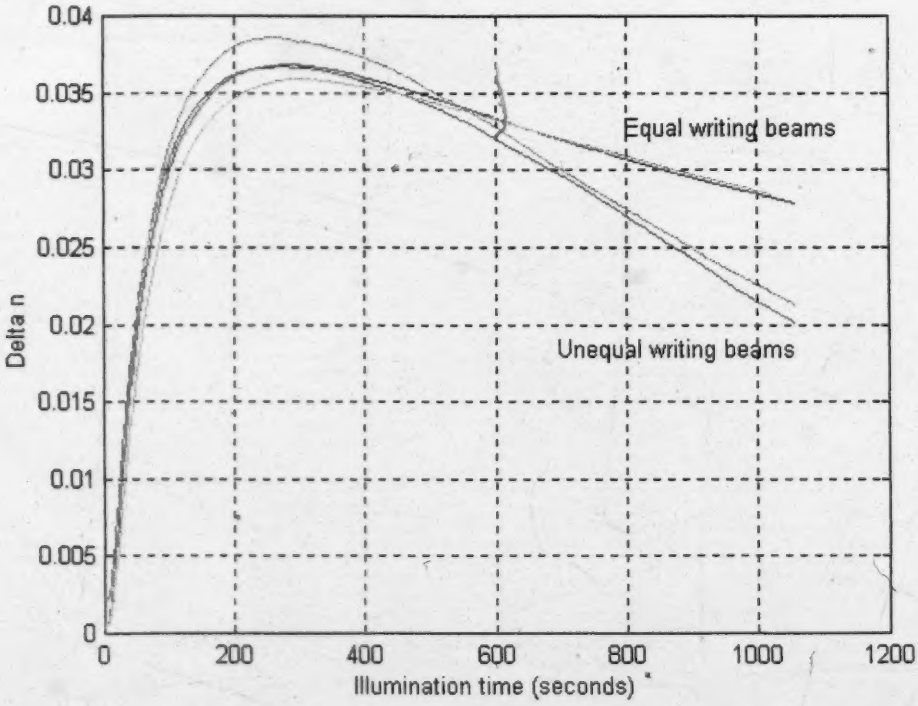

Figure 4.12. Graphs of Δn versus illumination time comparing gratings written with unequal and equal writing beam powers.

4.5 Thermal and Illumination related degradation of photo-induced gratings

The long term stability of the gratings was difficult to monitor due to the sensitivity and precision required of the diffraction experiment. Several contributing factors in the measurement of diffraction efficiency could change over the period of several months, days, or even hours, or were hard to reproduce from one experiment to the next. These factors include temperature fluctuations and vibrations over the short term. The most critical long term variable was the exact positioning of the probe beam at the center of a given grating, which was difficult to reproduce once the sample had been moved. However, an attempt was made to monitor longer term grating stability. After a period of two months, all diffraction efficiencies were within 0.1% of their initial reading. This can be seen by the graph in Figure 4.13, which studied a grating over 6 weeks. Some efficiencies were even slightly above their initial readings, which displays how difficult it is to precisely record the gratings over an extended period of time.

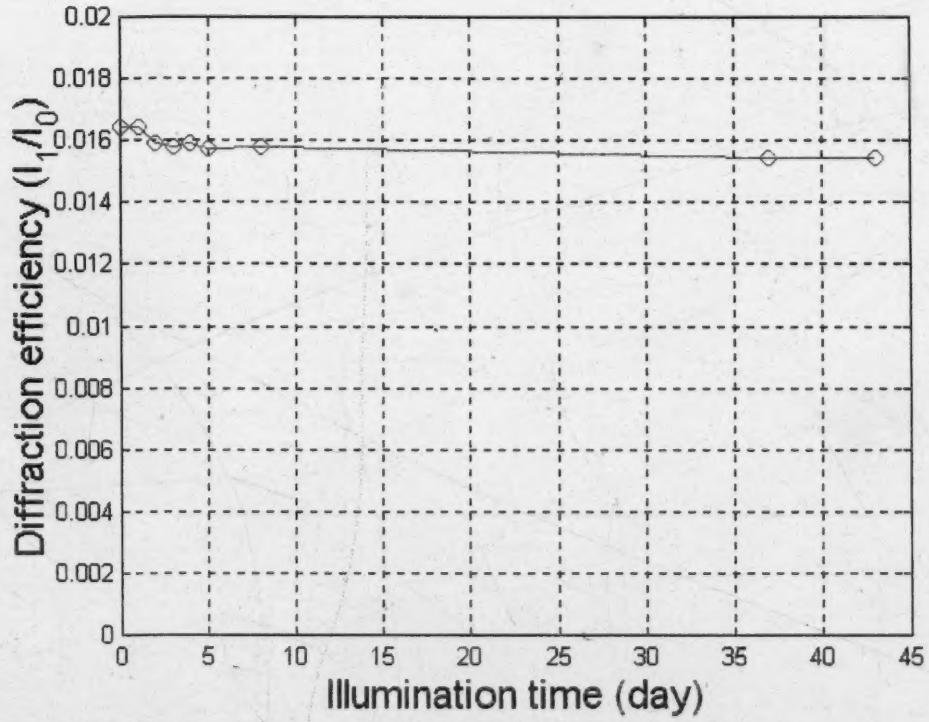

Figure 4.13. Diffraction efficiency graph with points taken over a period of 6 weeks.

It does appear that with a 9.6 mW laser, and an exposure energy of ~100 mJ/mm^2, the gratings produced are relatively stable. Gratings that were flood exposed to a high intensity white light did show a significant drop in grating efficiency. In those cases, the entire region under white illumination was visibly photodarkened, and the index contrast was presumably erased in the process.

To illustrate the effect that the high intensity white light has on grating strength, a grating was produced on a thin film with prior white light photodarkening present. Figure 4.14 compares diffraction efficiency graphs due to two gratings on the same film sample. One grating was on unexposed glass, the other grating was on a white light exposed section of the glass.

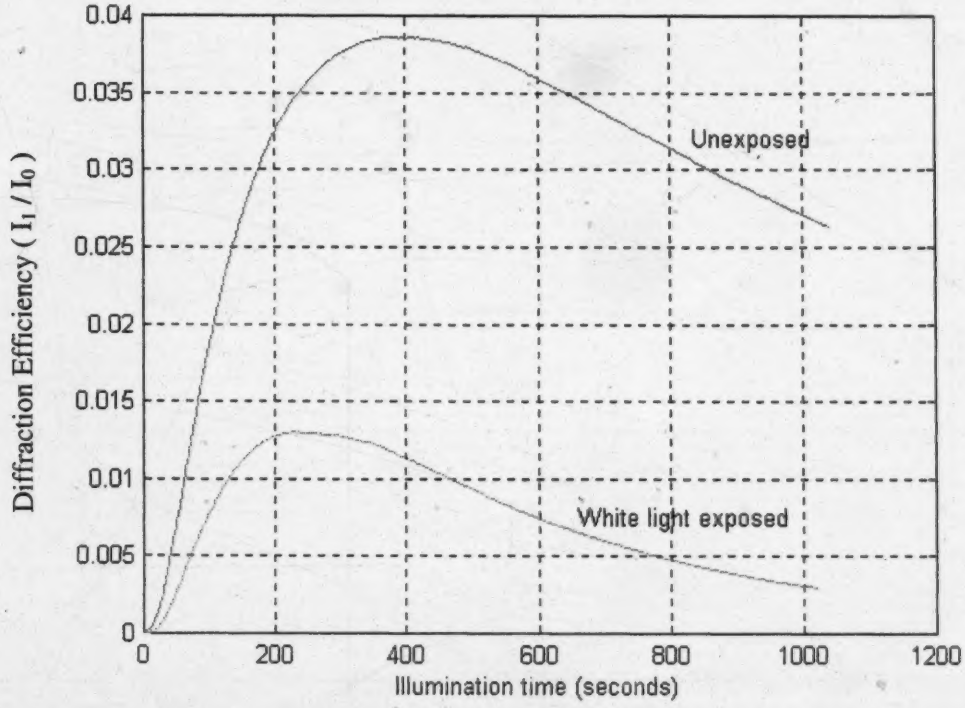

Figure 4.14. Diffraction efficiency graph comparing gratings written on high intensity white light photodarkened glass and unexposed glass.

We conclude that white light can cause enough photodarkening to affect grating quality. Although the white light used was extremely high intensity, it is still recommended to

keep any chalcogenide glass to be used in grating production in the dark, and any components in an enclosed package.

4.6. Verification of Assumptions

Diffraction efficiency calculations detailed in Chapter 3 were for the general case of mixed gratings, i.e. consisting of both refractive index and absorption changes. Equations (3.23 and 3.24) are repeated here.

$$\frac{I_0}{I_i} = \exp\left(\frac{-\alpha z}{\cos\gamma}\right)\left[\cos^2\left(\frac{\pi\Delta n z}{\lambda\cos\gamma}\right) + \cosh^2\left(\frac{\Delta\alpha z}{4\cos\gamma}\right) - 1\right] \tag{3.22}$$

$$\frac{I_1}{I_i} = \exp\left(\frac{-\alpha z}{\cos\gamma}\right)\left[\sin^2\left(\frac{\pi\Delta n z}{\lambda\cos\gamma}\right) + \sinh^2\left(\frac{\Delta\alpha z}{4\cos\gamma}\right)\right] \tag{3.23}$$

It was assumed that the contribution due to an absorption change was negligible in the gratings, when compared to the contribution due to the refractive index change. Therefore when (3.23) is divided by (3.22) the simple diffraction efficiency equation (3.24) is formed.

$$\eta = \frac{I_1}{I_0} = \tan^2\left(\frac{\pi\Delta n z}{\lambda\cos\gamma}\right) \tag{3.24}$$

The assumption of a negligible absorption change can now be verified. As a conservative estimate, assume that the absorption constant itself is the upper limit to the change of the absorption coefficient. As an example, consider the representative values $\Delta n = 0.037$, $z = 1.18\mu m$, $\lambda = 839nm$, and $\gamma = 15.11°$, corresponding to the results shown in Figures 4.2 to 4.4. Conservatively let $\Delta\alpha = \alpha = 3\times10^5\ m^{-1}$ (as shown in figure 4.9). The refractive index term and absorption coefficient terms of equation (3.22) are then $\cos^2[(\pi*\Delta n*z)/(\lambda*\cos\gamma)] = 0.972$, and $\cosh^2[(\Delta\alpha*z)/(4*\cos\gamma)] - 1 = 0.008$ respectively. Also the refractive index term and absorption coefficient terms of equation (3.23) are then $\sin^2[(\pi*\Delta n*z)/(\lambda*\cos\gamma)] = 0.028$, and $\sinh^2[(\Delta\alpha*z)/(4*\cos\gamma)] = 0.008$. The terms containing Δk are negligible compared to the terms containing Δn, confirming our assumption that led to equation (3.24).

The coupled wave theory described in Chapter 3 and above require an assumption of thick holographic gratings. One measure of grating thickness is given by the parameter,

$$Q = \frac{2\pi\lambda z}{n\Lambda^2} . \qquad (4.3)$$

The grating is assumed thick when Q>>1, and it is recommended that when Q = 10, coupled wave theory begins to gives good results [67]. Using λ = 839 nm, z = 1.18 μm, n = 2.87, Λ = 0.56 μm, corresponding to the grating shown in Figures 4.2 to 4.4, results in Q = 6.9. This is a little below the recommended thickness above which coupled wave theory is valid. Keeping everything but thickness constant in equation (4.3), the thickness required to obtain Q = 10 is z = 1.71 μm. The gratings used in Figures 4.5 and 4.6 had thicknesses around 2.2 μm, and were thus above the required thickness. These gratings produced refractive index data similar to the earlier thinner ones. We therefore can assume that coupled wave theory was a reasonably valid approximation for analyzing the experimental gratings.

Finally, the coupled wave theory implicitly assumes that a grating is uniform and extends throughout the thickness of the ChG film. This is not rigorously true, since the writing beam intensity falls (due to photon absorption in the ChG) with distance below the surface of the film. Figure 4.9 shows that the absorption coefficient of As_2Se_3 at the illumination wavelength of 633 nm is around $1.5 \times 10^6 m^{-1}$. This implies an absorption length of 0.67μm where 63% of the energy is absorbed. After this thickness, the next two absorption lengths absorb 32% of the remaining 37% of energy. This implies that the gratings created are not uniform throughout the entire thickness of the glass, but this was assumed so for samples less than three absorption lengths in thickness.

4.7. Error Analysis

The grating's refractive index modulation equation (4.2) used throughout this thesis is dependant on η (the diffraction efficiency), z (the thickness of the film), λ (the probe wavelength), and γ (the angle of probe incidence).

$$\Delta n = \text{atan}\left(\sqrt{\eta}\right)\left(\frac{\lambda \cos\gamma}{\pi z}\right) \qquad (4.2)$$

Error in any, of these measured parameters affects the accuracy of the estimated refractive index modulation. Given the values of $\eta = 0.025$, $z = 1.2 \times 10^{-6}$m, $\lambda = 839 \times 10^{-6}$m, and $\gamma = 15°$, the refractive index modulation calculated is 0.0337. An error in diffraction efficiency may arise from inaccuracy of the two power meters. An error of 3% in each power meter gives a diffraction efficiency error of 6%($\eta = 0.0265$), which results in Δn being 0.0347. This is an error of 2.9%. An error in film thickness, z, would arise due to inaccuracy of the profilometer, which is accurate to $\pm 0.01\mu$m. A film thickness of 1.21μm would result in Δn calculated to be 0.0334. This is an error of 0.9%. Lastly, an error might arise from the angle of the probe beam, which is changed manually. If this value is incorrect by 1°, i.e.$\gamma = 16°$, then $\Delta n = 0.0335$. This is an error of 0.6%. Thus, it is estimated that the refractive index as stated is accurate within approximately ± 5%

Chapter 5

Discussion and Future Work

5.1. Discussion

This thesis detailed the results of using an interferometric setup to create strong sub-micron Bragg gratings in thermally evaporated non-annealed As_2Se_3 thin films. A Helium-Neon laser was used as the illumination source, which has a wavelength of 633 nm and a photon energy of 1.96 eV. This illumination energy is above the band-gap of this particular glass (1.76eV). The refractive index change measured in the gratings were as large as 0.036. The refractive index of a-As_2Se_3 at the wavelength 1550nm is 2.73, therefore the gratings contain a change of 1.3 % in the refractive index. The gratings induced by this method had periods as small as 0.56 μm.

There is still much work to be done in studying As_2Se_3 gratings, as well as other ChG gratings. It would be quite useful to extensively study the grating stability as a function of heat and time. In the short term, it appeared the gratings were stable, but more thorough investigation on this will need to be done.

Also, further study on gratings induced by different wavelengths of light will be useful. We have demonstrated gratings created in As_2Se_3 using green (λ = 594 nm) and yellow (λ = 544 nm) lasers, but detecting them was difficult. There is a need for a comparison between different gratings created from different laser sources. Future studies should also include a study of the laser intensity on the creation of gratings.

Besides As_2Se_3 (studied here) and As_2S_3 (studied by numerous other groups), there are still many ChG alloys which have not been examined. The photodarkening characteristics of all ChGs will be useful in the future, as well as other induced effects. The degree of these effects appear to differ for each ChG, and are dependant on different

factors (band-gap, wavelength, intensity, etc.). A detailed study of each glass compound would be beneficial to future researchers, as each effect in each glass may have technological potential.

One of the reasons that the work of this thesis was undertaken was for potential application in integrated optics (IO). We have utilized the characteristics of photodarkening to induce Bragg gratings, but the refractive index modulation that occurs during photodarkening is also useful in other passive devices such as waveguides. Several other characteristics of ChG enhance its ability to be used in both active and passive devices. ChG has displayed large Kerr coefficients [10], and has been doped by rare-earth elements [11]. Thus they may also be used in switching and amplifier devices. They may also be deposited at room temperature, which allows deposition without subjecting the substrate to extreme temperatures. Other than photodarkening, several other photoinduced properties have also been mentioned in this thesis, which may be of technological importance. It is the culmination of all of these properties and characteristics that lead us to believe that ChG is an extremely useful integrated optical material of the future.

References

[1] G. P. Agrawal, *Fiber-Optic Communication Systems*, Wiley-Interscience, 1997.

[2] Statistics Canada Website: http://strategis.ic.gc.ca/epic/internet/inict-tic.nsf/vwGeneratedInterE/h_it06155e.html

[3] T. Miya, "Silica-based planar lightwave circuits: passive and thermally active devices", *IEEE Journal of Selected Topics in Quantum Electronics*, vol. 6, no. 1,pp. 38-45, January/February 2000.

[4] A. G. Rickman, G. T. Reed, F. Namavar, "Silicon-on-insulator optical rib waveguide circuits for fiber optic sensors", *Proceedings of the SPIE*, vol. 2071, pp. 190-196, December 1993.

[5] R. K. Watts, M. deWit, W. C. Holton, "Nonoxide Chalcogenide Glass Films for Integrated Optics", *Applied Optics*, vol. 13, no. 10, pp. 2329-2332, October 1974.

[6] T. Schweizer, D. W. Hewak, D. N. Payne, T. Jensen, and G. Huber, "Rare-earth doped chalcogenide glass laser", *Electronics Letters*, vol. 32, no. 7, pp. 666-667, March 1996.

[7] J. Kirchhof, J. Kobelke, M. Sheffler, and A. Schwuchow, "As-S based materials and fibres towards efficient 1.3 μm fibre amplification", *Electronics Letters*, vol 32, no. 13, pp. 1220-1221, June 1996.

[8] M. Asobe, T. Ohara, T. Kaino, and I. Yokohama, "Low power all-optical switching in a nonlinear optical loop mirror using chalcogenide glass fibre", *Electronics Letters*, vol. 32, no. 15, pp. 1396-1397, July 1996.

[9] J. F. Viens, C. Meneghini, A. Villeneuve, T. V. Galstian, E. J. Knystautas, M. A. Duguay, K. A. Richardson, and T. Cardinal, "Fabrication and characterization of integrated optical waveguides in sulfide chalcogenide glasses", *IEEE Journal of Lightwave Technology*, vol. 17, no. 7, pp. 1184-1191, July 1999.

[10] J. M. Harbold, F. O. Ilday, F. W. Wise, J. S. Sanghera, V.Q. Nguyen, L. B. Shaw, and I. D. Aggarwal, "Highly nonlinear As-S-Se glasses for all-optical switching", *Optics Letters*, vol. 27, no. 2, pp. 119-121, January 2002.

[11] S. Q. Gu, S. Ramachandran, E. E. Reuter, D. A. Turnbull, J. T. Verdeyen, S. G. Bishop, "Novel broad-band excitation of Er^{3+} luminescence in chalcogenide glasses", *Applied Physics Letters*, vol. 66, no. 6, pp. 670-672, February 1995.

[12] A. Madan, M. P. Shaw, *The Physics and Applications of Amorphous Semiconductors*, Academic Press, 1988.

[13] J. Tauc, *Amorphous and Liquid Semiconductors*, Plenum, 1974.

[14] N. F. Mott, E. A. Davis, *Electronic Processes in Non-Crystalline Materials*, Clarendon Press, 1979.

[15] J. Viens, C. Meneghini, A. Villeneuve, T. Galstian, E. J. Knystautas, M. A. Duguay, K. A. Richardson, T. Cardinal, "Fabrication and Characterization of Integrated Optical Waveguides in Sulfide Chalcogenide Glasses", *IEEE Journal of Lightwave Technology*, vol. 17, no. 7, pp-1184-1191, July 1999.

[16] K. Tanaka, Y. Ohtsuka, "Photo-induced Optical Changes in Amorhous As-S Films", *Thin Solid Films*, vol. 48, pp. 17-26, 1978.

[17] S. A. Keneman, "Hologram Storage in Arsenic Trisulfide Thin Films", *Applied Physics Letters*, vol. 19, no. 6, pp. 205-207, September 1971.

[18] J. S. Berkes, W. I. Samuel Jr., J.H. William, "Photodecomposition of Amorphous As_2Se_3 and As_2S_3", *Journal of Applied Physics*, vol. 42, no. 12, pp. 4908-4916, November 1971.

[19] J. P. DeNeufville, S.C. Moss, S. R. Ovshinsky, "Photostructural Transformations in Amorphous As_2Se_3 and As_2S_3 Films", *Journal of Non-Crystalline Solids*, vol. 13, pp. 191-223, 1973.

[20] H. Hamanaka, K. Tanaka, S. Iizima, "Reversible Photostructural Change in Melt-Quenched As_2S_3 Glass", *Solid State Communications*, vol. 23, pp. 63-65, 1977.

[21] K. Tanaka, "Reversible Photostructural Change: Mechanisms, Properties and Applications", *Journal of Non-Crystalline Solids*, vol. 35 & 36, pp. 1023-1034, 1980.

[22] K. Tanaka, H. Hisakuni, "Photoinduced Phenomena in As_2S_3 Glass Under Sub – Bandgap Excitation", *Journal of Non-Crystalline Solids*, vol. 198-200, pp. 714-718, 1996.

[23] K. Tanaka, "Configurational and Structural Models for Photodarkening in Glassy Chalcogenides", *Japanese Journal of Applied Physics*, vol. 25, no. 6, pp. 779-786, June 1986.

[24] M. Okuda, T. T. Nang, T.Matsushita, "Photo-Induced Absorption Changes in Selenium-Based Chalcogenide Glass Films", *Thin Solid Films*, vol. 58, pp. 403-406, 1979.

[25] T. Igo, Y. Toyoshima, "A Reversible Optical Change in the As-Se-Ge Glass", *Journal of Non-Crystalline Solids*, vol. 11, pp. 304-308, 1973.

[26] S. Rajagopalan, K.S. Harshavardhan, L. K. Malhotra, K. L. Chopra, "Photo-optical Changes in Ge-Chalcogenide Films", *Journal of Non-Crystalline Solids*, vol. 50, pp. 29-38, 1982.

[27] V. L. Averyanov, A.V. Kolobov, B. T. Kolomiets, V. M. Lyubin, "A Model of Photostructural Changes in Chalcogenide Vitreous Semiconductors: 2. Experimental Results", *Journal of Non-Crystalline Solids*, vol. 45, pp. 343-353, 1981.

[28] J. Z. Liu, P. C. Taylor, "Absence of Photodarkening in Bulk, Glassy As2S3 and As2Se3 Alloyed with Copper", *Physical Review Letters*, vol 59, no. 17, pp. 1938-1941, October 1987.

[29] K. Hayashi, N. Mitsuishi, "Thickness effect of the photodarkening in amorphous chalcogenide films", *Journal of Non-Crystalline Solids*, vol. 299-302, pp. 949-952, 2002.

[30] Y. Isbi, S. Sternklar, E. Granot, V. Lyubin, M. Klebanov, A. Lewis, "Sub-wavelength optical recording on chalcogenide glassy film", *Optics Communications*, vol. 171, pp. 219-223, December 1999.

[31] K. Tanaka, "Reversible photoinduced change in intermolecular distance in amorphpous As_2S_3 network", *Applied Physics Letters*, vol. 26, no. 5, pp. 243-245, March 1975.

[32] E. Mytilineou, P. C. Taylor, E. A. Davis, "On the Absence of Photodarkening in Pnictide Amorphous Semiconductors", *Solid State Communication*, vol. 35, pp. 497-499, 1980

[33] C. Y. Yang, M. A. Paesler, and D. E. Sayers, "Measurement of local structural configurations associated with reversible photostructural changes in arsenic trisulfide films", *Physical Review B*, vol. 36, no. 17, pp. 9160-9167, December 1987.

[34] K. Tanaka, Y Ohtsuka, "Measurements of photoinduced transformations in amorphous As2S3 films by optical waveguiding", *Journal of Applied Physics*, vol. 49, no. 12, pp. 6132-6135, December 1978.

[35] A. C. vanPopta, R. G. DeCorby, C. J. Haugen, T. Robinson, J. N. McMullin, D. Tonchev, S. O. Kasap, "Photoinduced refractive index changes in As2Se3 by 633nm illumination", *Optics Express*, vol. 10, no. 15, pp.639-644, July 2002.

[36] K. Tanaka, Y. Ohtsuka, "Composition Dependence of Photo-induced Refractive Index Changes in Amorphous As-S Films", *Thin Solid Films*, vol. 57, pp. 59-64, 1979.

[37] J. Dikova, P. Sharlandjiev, P. Gushterova, T. Babeva, "Photoinduced changes in the optical properties of obliquely deposited a-As_2S_3 thin films", *Vacuum*, vol. 69, pp. 395-398, 2003.

[38] R. A. Street, T. M. Searle, I. G. Austin, "Photoluminescence in amorphous As_2S_3", *Journal of Physics C: Solid State Physics*, vol. 6, pp. 1830-1840, 1973.

[39] F. Mollot, J. Cernogora, C. Benoit à la Guillaume, "Study of Localized States in Amorphous Semiconductor Chalcogenides by Radiative Recombination", *Physica Status Solidi (A) Applied Research*, vol.21, pp. 281-289, 1974.

[40] T. Tada, T. Ninomiya, "Photoluminescence from Optically Induced Metastable States in a-As2S3", *Journal of Non-Crystalline Solids*, vol. 11, pp. 88-90, 1989.

[41] K. Shimakawa, "Persistent photocurrent in amorphous chalcogenides", *Physical Review B*, vol. 34, no. 12, pp. 8703-8708, December 1986.

[42] K. Shimakawa, A. Kondo, K. Hayashi, S. Akahori, T. Kato, "Photoinduced metastable defects in amorphous semiconductors: communality between hydrogenated amorphous silicon and chalcogenides", *Journal of Non-Crystalline Solids*, vol. 174-166, pp. 387-390, 1993.

[43] V. M. Lyubin, V. L. Averyanov, B. T. Kolomiets, M. A. Taguirdzhanov, *Amorphous Semiconductors*, Publishing House of the Hungarian Academy of Sciences, 1976.

[44] K. Shimakawa, S. R. Elliott, "Reversible photoinduced change of ac conduction in amorphous As2S3 films", *Physical Review B*, vol. 38, no. 17, pp. 12479-12482, 1988.

[45] V. G. Zhdanov, B. T. Kolomiets, V. M. Lyubin, V. K. Malinovskii, "Photoinduced Optical Anisotropy in Chalcogenide Vitreous Semiconducting Films", *Physica Status Solidi (A) Applied Research*, vol. 52, pp. 621- 626, 1979.

[46] V. M. Lyubin, V. K. Tikhmirov, "Photodarkening and Photoinduced Anisotropy in Chalcogenide Vitreous Semiconductor Films", *Journal of Non-Crystalline Solids*, vol. 114, pp. 133-135, 1989.

[47] J. Hajto, G. Zentai, I. Koisa Somogyi, "Light-Induce Transmittance Oscillation in $GeSe_2$ Thin Films", *Solid State Communications*, vol. 23, pp. 401-403, 1977.

[48] S. R. Elliot, A. V. Kolobov, "A thermal light-induced vitrification of As50Se50 films", *Journal of Non-Crystalline Solids*, vol. 128, pp. 216-220, 1991.

[49] M. T. Kostyshin, E.V.Mikhailovskaja, P.F.Romanenko, "Photographic Sensitivity Effect in Thin Semiconducting Films on Metal Substrates", *Soviet Physics-Solid State*, vol.8, no. 2, pp.451-452, 1966.

[50] S. Maruno, T. Kawaguchi, "Metal photosurface deposition in As-S-Ag glasses", *Journal of Applied Physics*, vol. 46, no. 12, pp. 5312-5314, December 1975.

[51] H. Hamanaka, K. Tanaka, A. Matsuda, S. Iizima, "Reversible Photo-induced Volume Changes in Evaporated As_2S_3 and $As_4Se_5Ge_1$ Films", *Solid State Communications*, vol. 19, pp. 499-501, 1976.

[52] H. Hisakuni, K. Tanaka, "Giant photoexpansion in As_2S_3 glass", *Applied Physics Letters*, vol. 65, no. 23, pp. 2925-2927, December 1994.

[53] S. Ramachandran, J. C. Pepper, D. J. Brady, S. G. Bishop, "Micro-Optical Lenslets by Photo-Expansion in Chalcogenide Glasses", *Journal of Lightwave Technology*, vol. 15, no. 8, pp. 1371-1377, August 1997.

[54] L. K. Malhotra, A. Kumar, K. L.Chopra, "Photodensification in Amorphous P-Se Thin Films", *Thin Solid Films*, vol. 124, pp. 309-315, 1985.

[55] R. G. Brandes, F. P. Laming, A. D. Pearson, "Optically Formed Dielectric Gratings in Thick Films of Arsenic-Sulfur Glass", *Applied Optics*, vol. 9, no. 7, pp. 1712-1714, July 1970.

[56] A. M. Andriesh, Y. A. Bykovskii, E. P. Kolomeiko, A. V. Makovkin, V. L. Smirnov, A. V. Shmal'ko, "Waveguide structures and functional elements of integrated optics systems based on volume holographic gratings in thin As_2S_3 films", *Soviet Journal of Quantum Electronics*, vol. 7, no. 3, pp. 347-352, March 1977.

[57] T. Yaji, S. Kurita, "Amorphous As_2S_3 film waveguide with optical grating devices", *Optical Engineering*, vol. 20, no. 6, pp. 922-926, November-December 1981.

[58] K. Kase, G. C. Chern, I. Lauks, " Dry etching of gratings on spin-coated As_2S_3 films", *Thin Solid Films*, vol. 116, pp. L53-L54, 1984.

[59] K. Shiramine, H. Hisakuni, K. Tanaka, "Photoinduced Bragg reflector in As_2S_3 glass", *Applied Physics Letters*, vol. 64, no. 14, pp. 1771-1773, April 1994.

[60] K. Tanaka, N. Toyosawa, H. Hisakuni, "Photoinduced Bragg gratings in As_2S_3 optical fibers", *Optics Letters*, vol. 20, no. 19, pp. 1976-1978, October 1995.

[61] M. Asobe, T. Ohara, I. Yokohama, T. Kaino, "Fabrication of Bragg grating in chalcogenide glass fibre using the transverse holographic method", *Electronics Letters*, vol. 32, no. 17, pp. 1611-1613, August 1996.

[62] T. V. Galstyan, J. F. Viens, A. Villeneuve, K. Richardson, M.A. Duguay, "Photoinduced Self-Developing Relief Gratings in Thin Film Chalcogenide As_2S_3 Glasses", *IEEE Journal of Lightwave Technology*, vol. 15, no. 8, pp. 1343-1347, August 1997.

[63] A. Saliminia, A. Villeneuve, T. V. Galstyan, S. LaRochelle, K. Richardson, " First- and Second-Order Bragg Gratings in Single-Mode Planar Waveguides of Chalcogenide Glasses", *IEEE Journal of Lightwave Technology*, vol.17, no. 5, pp. 837-842, May 1999.

[64] M. Fischer, T. Galstian, R. Valle, A. Saliminia, "Surface and volume contributions to total diffractional efficiency in As_2S_3 thin film glasses", *Synthetic Metals*, vol. 127, pp. 303-306, 2002.

[65] T. Robinson, R. DeCorby, C. Haugen, J. McMullin, S. Bian, S. Kasap, D. Tonchev, "Photoinduced Bragg gratings in amorphous As_2Se_3 thin films", *SPIE Conference, Opto Canada 2002*, CA03-514.

[66] T. Robinson, R, DeCorby, J. McMullin, C. Haugen, S. Kasap, D. Tonchev, "Strong Bragg gratings photoinduced by 633-nm illumination in evaporated As_2Se_3 thin films", *Optics Letters*, vol. 28, no. 6, pp. 459-461, March 15, 2003.

[67] H. Kogelnik, "Coupled Wave Theory for Thick Hologram Gratings", *Bell System Technical Journal*, vol. 48, no. 9, November 1969.

[68] R. Swanepoel, "Determination of the thickness and constants of amorphous silicon", *Journal of Physics E: Scientific Instruments*, vol. 16, pp. 1214-1222, 1983.

Appendix A: Experimental Equipment

Equipment	Description	Manufacturer	Model
Writing Laser	10mW He-Ne(632.7nm)	Coherent	31-2082
Probe Laser	839 nm Semiconductor laser	TRLabs assembled	
Linear Polarizer	Visible light polarizer	Newport	10LP-VIS
Lens 1	Plano-concave, f = -50.2 mm	Newport	KPC040AR.14
Lens 2	Plano-convex, f = 200 mm	Newport	KPX106AR.14
Beam Splitter	Visible non-polarizing beamsplitter	Newport	10BC17MB.1
Mirrors	Broadband dielectric mirrors	Newport	10D20BD.1
Photodectors	Infrared germanium photodetectors	Newport	818-IR

Table A.1. List of optical equipment used in experiment.

Appendix B: Swanepoel method for determining refractive index of thin films

In [35] we reported that the refractive index of As_2Se_3 changed by as much as 0.05 or 2% when illuminated with a 10mW He-Ne laser. These measurements were conducted using the method Swanepoel proposed in 1983 [68], which allows $n(\lambda)$ and $\alpha(\lambda)$ to be de-embedded from a transmission spectrum of a thin film.

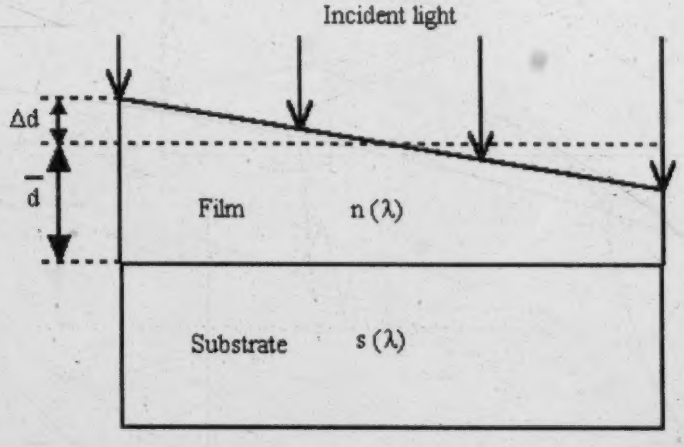

Figure A.1. Wedge shaped thin film model.

Figure 1 shows a model of the film and substrate. The film has a refractive index $\mathbf{n} = n-ik$, where k is the extinction coefficient. The coefficient of absorption of the film is $\alpha = 4\pi k/\lambda$. The substrate, which is transparent, has a refractive index s and is much thicker than the film. Both are surrounded by air, with the index of $n_0=1$. The films are assumed to be wedge shaped (which is a result of evaporating on a stationary substrate) to account for thickness non-umiformity, and have surface profiles described by

$$d=\bar{d}\pm\Delta d\,. \qquad (1)$$

Incident light from a spectrophotometer is used to collect a transmission spectrum for the samples, which will exhibit interference fringes. The basic equation for the interference fringes is

$$2nd=m\lambda\,, \qquad (2)$$

where m is an integer for each maximum (peak) and is a half integer for each minima (trough).

Using the transmission data, envelopes are created through the peaks and troughs. T_M will describe the peak envelope, and T_m will describe the trough envelope. In the highly transparent region ($n^2>>k^2$), absorption, α is assumed to be zero and the envelope equations can be written as,

$$T_M(\lambda)=\frac{\lambda}{2\pi n\Delta d}\frac{a}{(1-b^2)^{1/2}}\tan^{-1}\left[\frac{1+b}{(1-b^2)^{1/2}}\tan\left(\frac{2\pi n\Delta d}{\lambda}\right)\right] \quad (3)$$

$$T_m(\lambda)=\frac{\lambda}{2\pi n\Delta d}\frac{a}{(1-b^2)^{1/2}}\tan^{-1}\left[\frac{1-b}{(1-b^2)^{1/2}}\tan\left(\frac{2\pi n\Delta d}{\lambda}\right)\right] \quad (4)$$

where a = A/(B+D) and b = C/(B+D). A, B, C and D are denoted in [67] as $A = 16n^2s$, $B = (n+1)^3(n+s^2)$, $C = 2(n^2-1)(n^2-s^2)$, and $D = (n-1)^3(n-s^2)$.
Unique solutions for n and Δd may be found by solving Equations (3) and (4) simultaneously. Also, using Equation (2) for a pair of adjacent maxima or minima described by (n_1,λ_1) and (n_2,λ_2), Equation (5) may be used to find the average thin film thickness.

$$\overline{d}=\frac{\lambda_1\lambda_2}{2(\lambda_1 n_2-\lambda_2 n_1)} \quad (5)$$

Given the film's refractive index at each maximum and minimum value, a best fit line may be extrapolated to give n as a function of λ throughout the highly transmissive wavelength range. We limit our discussion to this range due to its usefulness in communication, but the envelope equations may be adjusted for more absorptive regions. The required equations for that case are discussed in [67].

After refractive index profiles are created for several chalcogenide samples, the glasses may be illuminated with band-gap light to induce refractive index changes. If the above method is applied to the illuminated samples, and compared with the original profiles, the degree of refractive index change may be analyzed.